

## Aminothiazoles as potent and selective Sirt2 inhibitors – a structure-activity relationship study

Matthias Schiedel, Tobias Rumpf, Berin Karaman, Attila Lehotzky, Judit Oláh, Stefan Gerhardt, Judit Ovádi, Wolfgang Sippl, Oliver Einsle, and Manfred Jung

*J. Med. Chem.*, **Just Accepted Manuscript** • DOI: 10.1021/acs.jmedchem.5b01517 • Publication Date (Web): 22 Dec 2015

Downloaded from <http://pubs.acs.org> on January 6, 2016

### Just Accepted

“Just Accepted” manuscripts have been peer-reviewed and accepted for publication. They are posted online prior to technical editing, formatting for publication and author proofing. The American Chemical Society provides “Just Accepted” as a free service to the research community to expedite the dissemination of scientific material as soon as possible after acceptance. “Just Accepted” manuscripts appear in full in PDF format accompanied by an HTML abstract. “Just Accepted” manuscripts have been fully peer reviewed, but should not be considered the official version of record. They are accessible to all readers and citable by the Digital Object Identifier (DOI®). “Just Accepted” is an optional service offered to authors. Therefore, the “Just Accepted” Web site may not include all articles that will be published in the journal. After a manuscript is technically edited and formatted, it will be removed from the “Just Accepted” Web site and published as an ASAP article. Note that technical editing may introduce minor changes to the manuscript text and/or graphics which could affect content, and all legal disclaimers and ethical guidelines that apply to the journal pertain. ACS cannot be held responsible for errors or consequences arising from the use of information contained in these “Just Accepted” manuscripts.



# Aminothiazoles as potent and selective Sirt2 inhibitors – a structure-activity relationship study

*Matthias Schiedel,<sup>†</sup> Tobias Rumpf,<sup>†</sup> Berin Karaman,<sup>#</sup> Attila Lehotzky,<sup>§</sup> Judit Oláh,<sup>§</sup> Stefan Gerhardt,<sup>||</sup> Judit Ovádi,<sup>§</sup> Wolfgang Sippl,<sup>#</sup> Oliver Einsle,<sup>||</sup> Manfred Jung<sup>†\*</sup>*

<sup>†</sup> Institute of Pharmaceutical Sciences, Albert-Ludwigs-University Freiburg, Albertstraße 25, 79104 Freiburg im Breisgau, Germany

<sup>#</sup> Institute of Pharmacy, Martin-Luther-University Halle-Wittenberg, Wolfgang-Langenbeck-Straße 4, 06120 Halle (Saale), Germany

<sup>§</sup> Institute of Enzymology, Research Centre for Natural Sciences, Hungarian Academy of Sciences, Magyar Tudósok körútja 2, H 1117 Budapest, Hungary

<sup>||</sup> Institute of Biochemistry and BIOSS Centre for Biological Signalling Studies, Albert-Ludwigs-University Freiburg, Albertstraße 21, 79104 Freiburg im Breisgau, Germany

KEYWORDS: epigenetics, histone deacetylases, sirtuins, inhibitors, drug design

1  
2  
3 ABSTRACT: Sirtuins are NAD<sup>+</sup>-dependent protein deacylases that cleave off acetyl, but also  
4 other acyl groups from the ε-amino group of lysines in histones and other substrate proteins.  
5  
6  
7  
8  
9  
10  
11  
12  
13  
14  
15  
16  
17  
18  
19  
20  
21  
22  
23  
24  
25  
26  
27  
28  
29  
30  
31  
32  
33  
34  
35  
36  
37  
38  
39  
40  
41  
42  
43  
44  
45  
46  
47  
48  
49  
50  
51  
52  
53  
54  
55  
56  
57  
58  
59  
60

Dysregulation of human Sirt2 (hSirt2) activity has been associated with the pathogenesis of cancer, inflammation, and neurodegeneration, which makes the modulation of hSirt2 activity a promising strategy for pharmaceutical intervention. The Sirtuin Rearranging Ligands (SirReals) have recently been discovered by us as highly potent and isotype-selective hSirt2 inhibitors. Here, we present a well-defined structure-activity relationship study, which rationalizes the unique features of the SirReals and probes the limits of modifications on this scaffold regarding inhibitor potency. Moreover, we present a crystal structure of hSirt2 in complex with an optimized SirReal derivative that exhibits an improved *in vitro* activity. Lastly, we show cellular hyperacetylation of the hSirt2 targeted tubulin caused by our improved lead structure.

1  
2  
3 INTRODUCTION: Until today, 18 different histone deacetylases (HDACs) have been  
4 identified and grouped into four classes, according to their homology to yeast HDACs, which  
5 were the first to be discovered.<sup>1</sup> Class I, II, and IV HDACs are Zn<sup>2+</sup>-dependent, while sirtuins,  
6 initially described as class III HDACs or Sir2 proteins, constitute a unique class of this enzyme  
7 super family. Sirtuins are dependent on NAD<sup>+</sup> as a cofactor to remove acetyl,<sup>2</sup> but also other acyl  
8 groups, such as myristoyl,<sup>3</sup> palmitoyl,<sup>4</sup> and succinyl,<sup>5</sup> from the ε-amino group of lysines. Beyond  
9 histones, a multitude of non-histone substrates has been identified in recent years, e.g. α-tubulin,<sup>6</sup>  
10 NFκB,<sup>7</sup> p53,<sup>8</sup> and BubR1.<sup>9</sup> Apart from deacylation, sirtuins were shown to catalyze ADP-  
11 ribosylation as well.<sup>10</sup> By regulating the acylation or ADP-ribosylation state of their substrate  
12 proteins, sirtuins have been implicated to influence a wide range of cellular processes like  
13 ageing,<sup>11</sup> metabolic sensing, apoptosis,<sup>12</sup> inflammation,<sup>13</sup> and transcription.<sup>14</sup> Sirtuins have been  
14 conserved from bacteria to eukaryotes and share a catalytic domain of approximately 260 amino  
15 acids with a high degree of sequence similarity. While bacteria and archaeobacteria possess only  
16 one or two sirtuins, in eukaryotes this number is higher. The human genome encodes seven  
17 sirtuin isotypes, which differ in their catalytic activity and their subcellular localization.<sup>15</sup> The  
18 human isotype Sirtuin 2 (hSirt2) is predominantly localized in the cytoplasm, however, it has  
19 also been found in the nucleus. hSirt2 was shown to have a major impact on cell cycle  
20 regulation,<sup>6</sup> peripheral myelination,<sup>16</sup> autophagy,<sup>17</sup> and immune and inflammatory response.<sup>18</sup> A  
21 dysregulation of hSirt2 activity was reported to play a critical role in the pathogenesis of  
22 cancer,<sup>19</sup> neurodegenerative diseases,<sup>20</sup> type II diabetes,<sup>21</sup> and bacterial infections.<sup>18b, 18c</sup> To  
23 further investigate the effects of hSirt2-dependent deacylation, and its impact on downstream  
24 signaling, modulators of hSirt2 activity are urgently needed. A number of hSirt2 modulators  
25 have been discovered thus far, and selected examples are depicted in Figure 1: the physiological  
26  
27  
28  
29  
30  
31  
32  
33  
34  
35  
36  
37  
38  
39  
40  
41  
42  
43  
44  
45  
46  
47  
48  
49  
50  
51  
52  
53  
54  
55  
56  
57  
58  
59  
60

1  
2  
3 sirtuin inhibitor nicotinamide (**1**)<sup>22</sup> and its derivatives 5-((5-benzamidonaphthalen-1-  
4 yl)oxy)nicotinamide (**2**)<sup>23</sup> and the 3'-phenethoxy-2-anilinobenzamide analogue **3**,<sup>24</sup> the highly  
5  
6 potent but unselective ELT inhibitor 31 (**4**),<sup>25</sup> the highly selective 5,6,7,8-  
7  
8 tetrahydrobenzo[4,5]thieno[2,3-d]pyrimidin-4(3H)-one (**5**),<sup>26</sup> AGK2 (**6**),<sup>27</sup> salermide (**7**),<sup>28</sup> and  
9  
10 the macrocyclic peptide S2iL5 (**8**).<sup>29</sup> However, isotype-selective and drug-like inhibitors of  
11  
12 hSirt2 with proven cellular activity are still scarce. Recently, we discovered a novel class of  
13  
14 potent and highly isotype-selective hSirt2 inhibitors.<sup>30</sup> Due to a major rearrangement of the  
15  
16 active site of hSirt2 upon ligand binding, these inhibitors were termed Sirtuin Rearranging  
17  
18 Ligands (SirReals). The core of the SirReals is an acylated 2-aminothiazole scaffold, which  
19  
20 connects an arylmethyl moiety with a 4,6-dimethylpyrimidine (Figure 1).  
21  
22  
23  
24  
25  
26  
27  
28  
29  
30  
31  
32  
33  
34  
35  
36  
37  
38  
39  
40  
41  
42  
43  
44  
45  
46  
47  
48  
49  
50  
51  
52  
53  
54  
55  
56  
57  
58  
59  
60

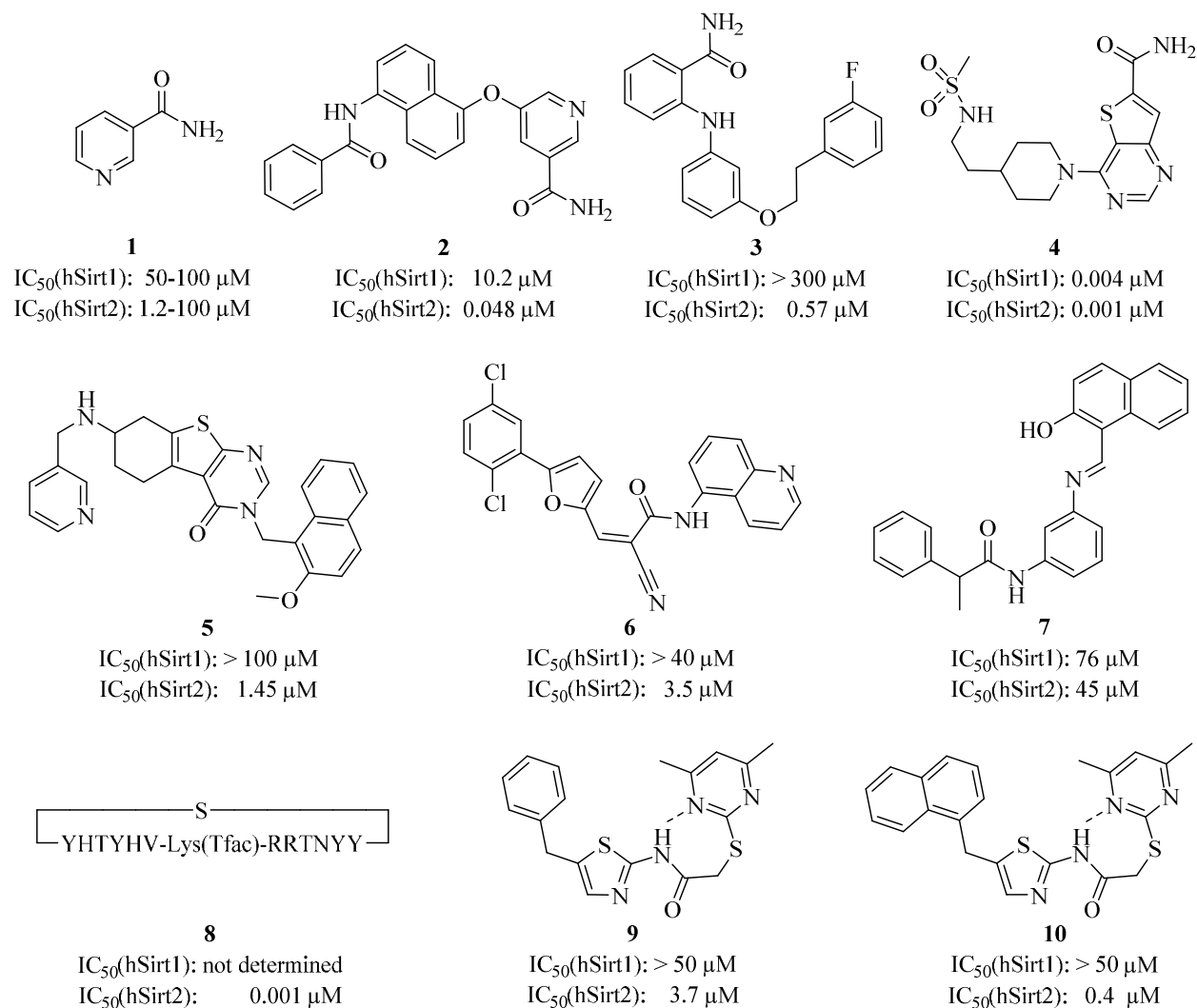


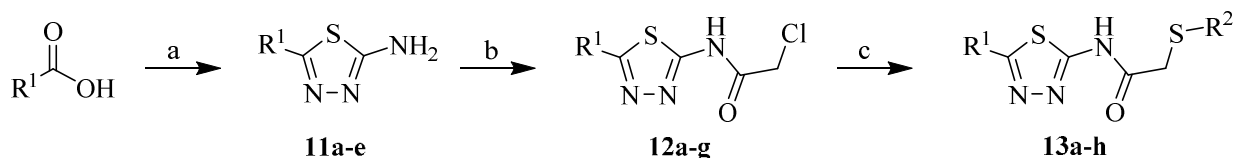
**Figure 1.** Chemical structures and inhibition data of selected hSirt2 inhibitors, including SirReal1 (**9**) and SirReal2 (**10**). The intramolecular hydrogen bonds are shown as dashed lines.

By inducing a rearrangement of the active site of hSirt2, the 4,6-dimethylpyrimidine moiety is bound to a yet-unexploited binding pocket, which lays the foundation for the excellent isotype-selectivity of the SirReals. Therefore, we named the newly formed binding site ‘selectivity pocket’. The arylmethyl moiety protrudes towards the substrate channel pushing the acyl-lysine out of its physiological position, and thereby enlarging the distance between substrate and NAD<sup>+</sup>. This efficiently blocks the acyl transfer. A preliminary structure activity relationship

(SAR) study has already been reported,<sup>30</sup> revealing an additive contribution of the arylmethyl and the 4,6-dimethylpyrimidine moiety, and the importance of the intramolecular hydrogen bond for activity. Here, we systematically probe further SARs to analyze the limits of modification within this scaffold.

RESULTS: Guided by the structural insights obtained from hSirt2-SirReal complexes,<sup>30</sup> we aimed to systematically probe the limits of variation within the scaffold of the SirReals and to establish a well-defined SAR-model. To study the effect of an alteration of the aminothiazole core, we initially generated a few synthetically easily accessible aminothiadiazole derivatives. The synthesis of these inhibitors is outlined in Scheme 1. A condensation of a carboxylic acid and thiosemicarbazide yielded the aminothiadiazoles **11a-e**,<sup>31</sup> which were subsequently chloroacetylated to obtain **12a-g**.<sup>32</sup> A reaction of the alkyl chlorides with aromatic thiols generated the desired aminothiadiazoles **13a-h** (Table 1).

**Scheme 1.** Synthesis of aminothiadiazoles<sup>a</sup>



<sup>a</sup>Reagents and conditions: (a) thiosemicarbazide, H<sub>2</sub>SO<sub>4</sub>, 80 - 90 °C, 7 h; (b) acetyl chloride, DIPEA, acetonitrile, 0 °C to rt, 2 h; (c) aromatic thiol, Na<sub>2</sub>CO<sub>3</sub>, KI, DMSO, 2 h.

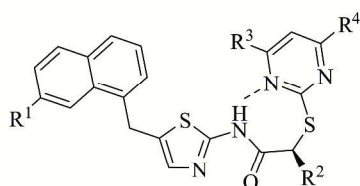
Our main focus was placed on the modifications of the arylmethyl and pyrimidine moieties, which were shown to be crucial for the interaction with the cofactor or ligand binding, respectively.<sup>30</sup> First, we explored modifications of the arylmethyl moiety. Molecular docking studies, based on the hSirt2-SirReal complexes,<sup>30</sup> indicated that substitutions at the naphthyl group of the parent compound **10** are beneficial for the potency of the ligands. Compound **14a**

1  
2  
3 (Figure 2a), a chloro-substituted derivative of the parent compound **10**, was predicted to interact  
4  
5 with the two backbone carbonyl groups of His187 and Val233 (Figure 2b). By means of a  
6  
7 halogenation of the naphthyl residue, we aimed to gain ligand affinity via a  $\sigma$ -hole interaction  
8  
9 with the peptide backbone. To follow up on this hypothesis we synthesized the halogenated  
10  
11 naphthyl derivatives **14a**, **14d**, **14f**, **14g**, **14i** (Table 2). Additionally, novel derivatives of the  
12  
13 parent compound **9**, with substituted benzyl moieties, were generated to consider the impact of  
14  
15 further structural changes of the arylmethyl moiety, as well. Encouraged by molecular docking  
16  
17 studies, that showed a high docking score for the (*S*)-enantiomer of **14b** (Figure 2a,c), we aimed  
18  
19 to synthesize SirReals with an additional alkylation in  $\alpha$ -position to the carbonyl of the amide  
20  
21 and eventually separated the enantiomers by chiral HPLC. The docking revealed that the methyl  
22  
23 group ((*S*)-configuration) is orientated towards the exit of the selectivity pocket, which can  
24  
25 accommodate longer alkyl groups. On the other hand, the (*R*)-configuration was predicted to be  
26  
27 less favorable due to the close proximity of the conserved water molecule and Ile93. This is also  
28  
29 reflected in the less favorable binding energies calculated for the (*R*)-enantiomer (Table S1).  
30  
31 Furthermore, we wanted to investigate the effects of structural changes of different substitution  
32  
33 patterns of the pyrimidine moiety. Initial structural data and SAR studies have shown that the  
34  
35 4,6-dimethylpyrimidine moiety perfectly fits into the newly formed ‘selectivity pocket’, and that  
36  
37 a loss of the methyl groups leads to a decay in ligand potency.<sup>30</sup> Additionally, molecular  
38  
39 docking, based on hSirt2-SirReal complexes,<sup>30</sup> demonstrated by the example of **14c** (Figure 2a),  
40  
41 that larger alkyl substituents, e.g. ethyl, in position 4 and 6 of the pyrimidine moiety cause a  
42  
43 steric clash with residues Ala135, Tyr139, and Leu206 of the ‘selectivity pocket’, as well as with  
44  
45 Thr171 of the C-pocket. These studies predicted a loss of the H-bond to the conserved water  
46  
47 molecule, and thereby lowering the ligand affinity to hSirt2 (Figure 2d). To show the accuracy of  
48  
49  
50  
51  
52  
53  
54  
55  
56  
57  
58  
59  
60



our docking studies we still wanted to actually test, whether hSirt2 would be able to accommodate its ‘selectivity pocket’ to other substitution patterns of the pyrimidine moiety, as well.

a

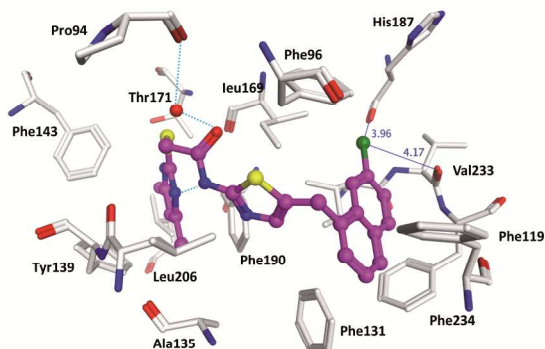


**14a** ( $R^1 = \text{Cl}$ ,  $R^2 = \text{H}$ ,  $R^3, R^4 = \text{CH}_3$ )

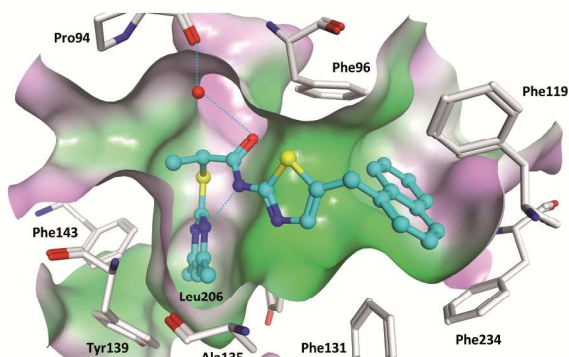
**(S)-14b** ( $R^1 = \text{H}$ ,  $R^2, R^3, R^4 = \text{CH}_3$ )

**14c** ( $R^1 = \text{H}$ ,  $R^2 = \text{H}$ ,  $R^3, R^4 = \text{C}_2\text{H}_5$ )

b



c



d

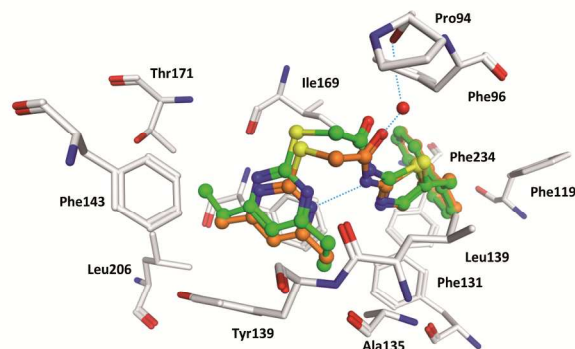
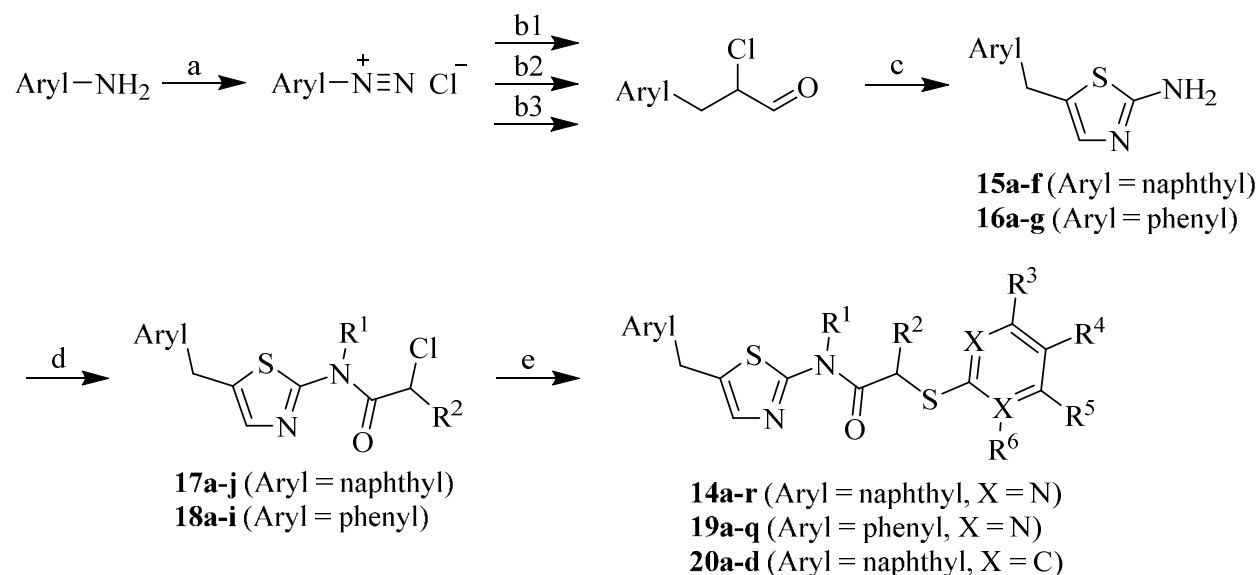


**Figure 2.** Docking poses derived for the envisaged SirReals **14a-c**. (a) Chemical structures used for docking studies. (b) Docking pose derived for **14a** (colored magenta). Distances between the halogen atom and the two carbonyl groups of His187 and Val233 are shown as blue lines with distances given in Angstrom. (c) Docking pose derived for *(S)*-**14b** (colored cyan). The methyl group (*(S)*-configuration) is orientated towards the exit of the ‘selectivity pocket’ which can accommodate longer alkyl groups. The molecular surface of the binding pocket is displayed and colored according to the hydrophobicity (green=hydrophobic, magenta= hydrophilic). (d) Docking pose derived for **14c** (colored green) in comparison with the X-ray structure of **10**

(colored orange). The larger ethyl groups of the pyrimidine ring cause steric clashes with Ala135 and Leu206 and, as a consequence, the H-bond to the conserved water molecules is lost. Hydrogen bonds are shown as dashed cyan colored lines, water molecules as red spheres.

To establish a well-defined SAR model, we set up a synthesis platform to generate a 2-aminothiazole library that was directed to yield compounds with a broad structural variety, particularly in the arylmethyl and pyrimidine parts of the ligand (Scheme 2).

**Scheme 2.** Synthesis platform utilized to generate the 2-aminothiazole library<sup>a</sup>



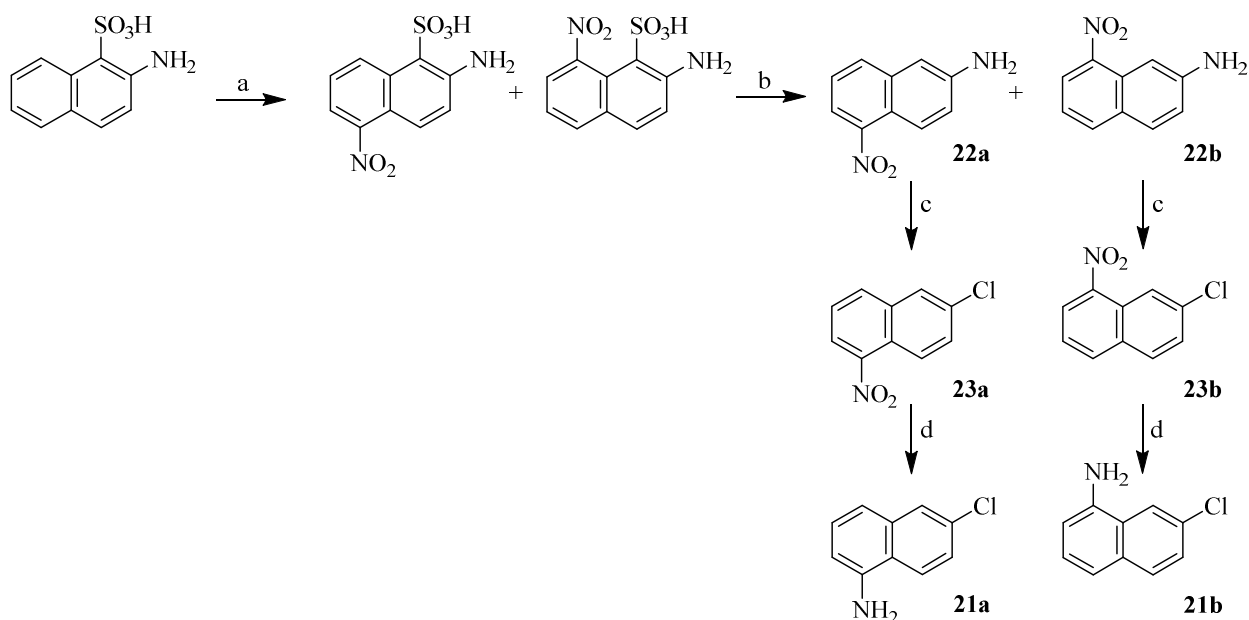
<sup>a</sup>Reagents and conditions: (a) NaNO<sub>2</sub>, HCl, water, -5 – 0 °C, 10 min; (b1) acrolein, CuCl<sub>2</sub> x 2 H<sub>2</sub>O, acetone, 3 h; (b2) NaHCO<sub>3</sub>, MgO; then acrolein, CuCl<sub>2</sub> x 2 H<sub>2</sub>O, acetone, 3 h; (b3) FeCl<sub>3</sub> x 6 H<sub>2</sub>O, HCl, water, -5 – 0 °C; then CuCl<sub>2</sub> x 2 H<sub>2</sub>O, HCl, acetone/ethanol, -5 – 0 °C; then acrolein, acetone/water, 4h; (c) thiourea or N-methylthiourea, ethanol, reflux, 2 h; (d) acyl chloride, DIPEA, acetonitrile, 0 °C to rt, 2 h; (e) aromatic thiol, Na<sub>2</sub>CO<sub>3</sub>, KI, DMSO, 2 h.

The biggest challenge within the synthesis of the SirReals was the preparation of  $\alpha$ -chloropropanals *via* Meerwein reaction,<sup>33</sup> due to the instability of some arenediazonium salts,

1  
2  
3 especially the naphthalenediazonium salts.<sup>34</sup> In order to overcome these issues, we had to use  
4  
5 three different methods to obtain sufficient amounts of the appropriate  $\alpha$ -chloropropanals.<sup>35</sup>  
6  
7 Toluene- and methoxybenzenediazonium salts could only be converted into the appropriate  $\alpha$ -  
8  
9 chloropropanals under standard Meerwein conditions in a neutral medium,<sup>35a</sup> while halogenated  
10  
11 benzenediazonium salts, as well as the diazonium salt from 4-phenylaniline, successfully reacted  
12  
13 in an acidic medium. For the synthesis of the 5-(naphthylmethyl)thiazol-2-amine derivatives  
14  
15 **15a-f**, we followed a modified version of the Meerwein reaction published by Obushak et al.<sup>35b</sup>  
16  
17 Initially, naphthalenediazonium chlorides were treated with iron(III) chloride in an aqueous  
18  
19 solution to obtain the naphthalenediazonium tetrachloroferrates(III). An exchange reaction with  
20  
21  $\text{CuCl}_2$  in acetone resulted in the precipitation of the naphthalenediazonium  
22  
23 tetrachlorocuprates(II), which were isolated and used as a fine crystalline powder for the  
24  
25 subsequent reaction with acrolein.<sup>35b</sup> With this protocol, we were able to generate the desired  
26  
27 naphthyl derivatives **15b-c**, which could not be synthesized under standard Meerwein conditions,  
28  
29 neither in an acidic nor in a neutral medium. For those naphthylamines that could be transformed  
30  
31 into the corresponding  $\alpha$ -chloropropanals using standard Meerwein conditions to a small  
32  
33 extent,<sup>35a</sup> the modified version of the Meerwein reaction enabled us to increase the yield of this  
34  
35 reaction largely. However, due to the time-consuming protocol of the modified Meerwein  
36  
37 reaction, it was exclusively used to synthesize the naphthyl derivatives **15a-f** and compound **16g**,  
38  
39 which could not be generated in satisfying yields applying standard Meerwein conditions. The  
40  
41  $\alpha$ -chloropropanals were immediately converted into the aminothiazole scaffold (**15a-f**, **16a-g**) by  
42  
43 condensation with thiourea.<sup>35a</sup> The aminothiazoles were subsequently chloroacetylated<sup>32</sup> to yield  
44  
45 **17a-j** and **18a-i**, followed by a nucleophilic substitution with an aromatic thiol to generate  
46  
47 compounds **14a-r**, **19a-q** and **20a-d**. The synthesis of the halogenated 1-naphthylamines (**21a-c**),  
48  
49  
50  
51  
52  
53  
54  
55  
56  
57  
58  
59  
60

which were needed as starting materials for the synthesis of the halogenated inhibitors (**14a**, **14d**, **14f**, **14g**, **14i**), is illustrated in Scheme 3 by the example of the chlorinated 1-naphthylamines **21a-b**. Starting with the nitration of 2-aminonaphthalene-1-sulfonic acid followed by a desulfonation<sup>36</sup> the isomers of the respective nitronaphthalenamines **22a-b** were separated by flash chromatography. Halonitronaphthalenes **23a-c** were synthesized by applying Sandmeyer conditions.<sup>37</sup> Finally, the halogenated 1-naphthylamines **21a-c** were obtained by a reduction of the nitro group with SnCl<sub>2</sub>.

**Scheme 3.** Synthesis of chlorinated 1-naphthylamines as starting material for further syntheses<sup>a</sup>

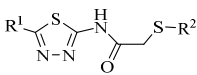
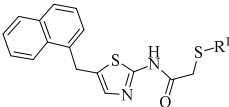
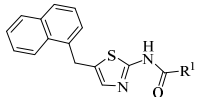
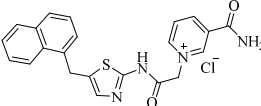
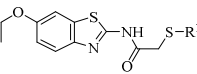
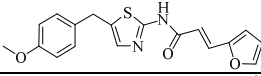
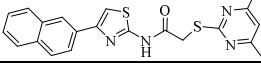
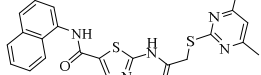


<sup>a</sup>Reagents and conditions: (a) H<sub>2</sub>SO<sub>4</sub>, KNO<sub>3</sub>, -15 °C, 40 min; (b) H<sub>2</sub>SO<sub>4</sub>/water (1:1), reflux, 40 min; (c) glacial acid, H<sub>2</sub>SO<sub>4</sub>, NaNO<sub>2</sub>, 15-20 °C, 15 min; then CuCl and HCl, rt, 1 - 4 h; (d) SnCl<sub>2</sub> x 2 H<sub>2</sub>O, ethanol, rt, 4 - 24 h.

The synthesized SirReal derivatives were evaluated for their inhibitory activity against hSirt1 and hSirt2 in a biochemical *in vitro* assay that was previously described.<sup>38</sup> The *in vitro* inhibition

data of the aminothiadiazoles (**13a-h**) and the aminothiazole derivatives **20a-d**, **24a-b**, **25**, **26a-b** and **27-32**, which strongly deviate from the original scaffold is summarized in Table 1. Aminothiazoles (**9-10**, **14a-r**, **19a-q**) and their *in vitro* inhibition of hSirt1 and hSirt2 are shown in Table 2.

**Table 1.** *In vitro* inhibition of hSirt1 and hSirt2 by aminothiadiazoles **13a-h** and aminothiazoles **20a-d**, **24a-b**, **25**, **26a-b** and **27-32**

Shared scaffold or complete chemical structure	compd	R <sup>1</sup>	R <sup>2</sup>	hSirt1 inhibition %@conc. [μM] or IC <sub>50</sub> ± SE [μM]	hSirt2 inhibition %@conc. [μM] or IC <sub>50</sub> ± SE [μM]
	<b>13a</b>	1-naphthylmethyl	4,6-dimethylpyrimidin-2-yl	n.i. @ 200 μM <sup>c</sup>	1.89 ± 1.50
	<b>13b</b>	phenyl	5,6-diphenyl-1,2,4-triazin-3-yl	n.i. @ 200 μM	19.9 ± 31.7
	<b>13c</b>	4-chlorobenzyl	4,6-dimethylpyrimidin-2-yl	n.i. @ 200 μM	30.9 ± 20.5
	<b>13d</b>	4-bromobenzyl	4,6-dimethylpyrimidin-2-yl	n.i. @ 200 μM	167.7 ± 30.29
	<b>13e</b>	trifluoromethyl	4,6-dimethylpyrimidin-2-yl	12% @ 200 μM	502.8 ± 43.95
	<b>13f</b>	phenyl	4,6-dimethylpyrimidin-2-yl	n.i. @ 200 μM	19.9% @ 50 μM
	<b>13g</b>	benzyl	4,6-dimethylpyrimidin-2-yl	n.i. @ 200 μM	17.8% @ 50 μM
	<b>13h</b>	methyl	4,6-dimethylpyrimidin-2-yl	n.i. @ 200 μM	n.i. @ 50 μM
	<b>20a</b>	3-hydroxyphenyl		n.i. @ 200 μM	143 ± 27.4
	<b>20b<sup>a</sup></b>	3,5-dimethylphenyl		16% @ 200 μM	207 ± 27.4
	<b>20c</b>	2-aminophenyl		n.i. @ 200 μM	36% @ 50 μM
	<b>20d</b>	4-chlorophenyl		n.i. @ 200 μM	n.i. @ 50 μM
	<b>24a</b>	CH <sub>3</sub>		n.i. @ 200 μM	84% @ 500 μM n.i. @ 50 μM
	<b>24b</b>	C <sub>5</sub> H <sub>11</sub>		n.i. @ 200 μM	77% @ 500 μM 48% @ 50 μM n.i. @ 10 μM
	<b>25</b>			39% @ 200 μM	289 ± 127
	<b>26a</b>	4,6-dimethylpyrimidin-2-yl		16% @ 200 μM	77.8 ± 7.62
	<b>26b<sup>b</sup></b>	4-hydroxy-6-propyl-pyrimidin-2-yl		n.i. @ 200 μM	n.i. @ 50 μM
	<b>27</b>			28% @ 200 μM	18% @ 50 μM
	<b>28</b>			23% @ 200 μM	35% @ 50 μM
	<b>29</b>			n.i. @ 200 μM	33.0 ± 15.4

	<b>30</b>			n.i. @ 200 $\mu$ M	24% @ 250 $\mu$ M
	<b>31</b>			n.i. @ 200 $\mu$ M	n.i. @ 50 $\mu$ M
	<b>32</b>			n.i. @ 200 $\mu$ M	n.i. @ 50 $\mu$ M

<sup>a</sup>Compound previously published by our group<sup>30</sup>

<sup>b</sup>Sirtuin inhibitor presented by Kazantsev et al.<sup>39</sup>

<sup>c</sup>n.i.: inhibition @ conc. [ $\mu$ M] < 10%

Among the aminothiadiazoles, compound **13a**, bearing a 1-naphthylmethyl and a 4,6,-dimethylpyrimidine moiety, displays the most potent hSirt2 inhibition. This is consistent with the previously published SirReal-mediated inhibition of hSirt2.<sup>30</sup> However, a switch from the aminothiazole to the aminothiadiazole scaffold was shown to lead to a loss in potency, and was therefore not further investigated. Furthermore, we observed a substantial decrease in potency for those compounds that strongly deviate from the original scaffold (**20a-d**, **24a-b**, **25**, **26a-b** and **27-32**, Table 1). Thus, we hypothesize that the unique mechanism of SirReal-mediated hSirt2 inhibition is restricted to compounds that display a high extent of similarity to the parent compounds **9** or **10**. By disassembling our lead structure **10** into fragments (**24a**, **30-32**, Table 1), we clearly demonstrate that the presence of all three functional elements, namely: arylmethyl, aminothiazole, and 4,6-dimethylpyrimidine is crucial for efficient inhibition of hSirt2 activity.

Table 2. *In vitro* inhibition of hSirt1 and hSirt2 by aminothiazoles 9-10, 14a-r, 19a-q

Shared scaffold:								
compd	Aryl	R1	R2	R3	R4	R5	hSirt1 inhibition %@conc. [μM] or IC <sub>50</sub> ± SE [μM]	hSirt2 inhibition %@conc. [μM] or IC <sub>50</sub> ± SE [μM]
9 <sup>a</sup>	phenyl	H	H	CH <sub>3</sub>	H	CH <sub>3</sub>	15% @ 200 μM	3.75 ± 0.83
10 <sup>a</sup>	naphthalen-1-yl	H	H	CH <sub>3</sub>	H	CH <sub>3</sub>	n.i. @ 200 μM	0.44 ± 0.08
14a	7-chloronaphthalen-1-yl	H	H	CH <sub>3</sub>	H	CH <sub>3</sub>	29% @ 200 μM	0.18 ± 0.02
rac-14b	naphthalen-1-yl	H	CH <sub>3</sub>	CH <sub>3</sub>	H	CH <sub>3</sub>	17% @ 200 μM	0.42 ± 0.04
(S)-14b	naphthalen-1-yl	H	(S)-CH <sub>3</sub>	CH <sub>3</sub>	H	CH <sub>3</sub>	n.i. @ 200 μM	0.26 ± 0.03
(R)-14b	naphthalen-1-yl	H	(R)-CH <sub>3</sub>	CH <sub>3</sub>	H	CH <sub>3</sub>	n.i. @ 200 μM	9.77 ± 4.78
14c	naphthalen-1-yl	H	H	C <sub>2</sub> H <sub>5</sub>	H	C <sub>2</sub> H <sub>5</sub>	n.i. @ 200 μM	45.6 ± 24.6
14d	7-bromonaphthalen-1-yl	H	H	CH <sub>3</sub>	H	CH <sub>3</sub>	n.i. @ 200 μM <sup>b</sup>	0.21 ± 0.02
14e	2-methylnaphthalen-1-yl	H	H	CH <sub>3</sub>	H	CH <sub>3</sub>	n.i. @ 200 μM	0.31 ± 0.01
rac-14f	7-chloronaphthalen-1-yl	H	C <sub>2</sub> H <sub>5</sub>	CH <sub>3</sub>	H	CH <sub>3</sub>	n.i. @ 200 μM	0.32 ± 0.05
14g	6-chloronaphthalen-1-yl	H	H	CH <sub>3</sub>	H	CH <sub>3</sub>	20% @ 200 μM	0.48 ± 0.05
rac-14h	naphthalen-1-yl	H	C <sub>2</sub> H <sub>5</sub>	CH <sub>3</sub>	H	CH <sub>3</sub>	35% @ 200 μM	0.54 ± 0.06
rac-14i	7-chloronaphthalen-1-yl	H	CH <sub>3</sub>	CH <sub>3</sub>	H	CH <sub>3</sub>	n.i. @ 200 μM	0.54 ± 0.08
14j	naphthalen-1-yl	H	H	CH <sub>3</sub>	H	H	n.i. @ 200 μM	1.45 ± 0.18
rac-14k	naphthalen-1-yl	H	CH <sub>3</sub>	H	H	H	21% @ 200 μM	1.92 ± 0.42
14l <sup>a</sup>	naphthalen-1-yl	H	H	H	H	H	17% @ 200 μM	2.34 ± 0.42
14m	naphthalen-1-yl	H	H	CH <sub>3</sub>	CH <sub>3</sub>	CH <sub>3</sub>	n.i. @ 200 μM	15.0 ± 2.11
14n	naphthalen-2-yl	H	H	CH <sub>3</sub>	H	CH <sub>3</sub>	n.i. @ 200 μM	65.0 ± 31.7
14o	naphthalen-1-yl	H	H	OH	H	C <sub>3</sub> H <sub>7</sub>	22% @ 200 μM	127.2 ± 13.4
14p <sup>a</sup>	naphthalen-1-yl	CH <sub>3</sub>	H	CH <sub>3</sub>	H	CH <sub>3</sub>	n.i. @ 200 μM	>100
14q	naphthalen-1-yl	H	H	OH	H	CH <sub>3</sub>	n.i. @ 200 μM	35% @ 50 μM
14r	naphthalen-1-yl	H	H	NH <sub>2</sub>	H	NH <sub>2</sub>	n.i. @ 200 μM	25% @ 50 μM
19a	3-ethoxyphenyl	H	H	CH <sub>3</sub>	H	CH <sub>3</sub>	n.i. @ 200 μM	1.33 ± 0.15
19b	3-methylphenyl	H	H	CH <sub>3</sub>	H	CH <sub>3</sub>	18% @ 200 μM	1.64 ± 0.40
19c	4-chlorophenyl	H	H	CH <sub>3</sub>	H	CH <sub>3</sub>	n.i. @ 200 μM	3.40 ± 0.49
19d	4-methylphenyl	H	H	CH <sub>3</sub>	H	CH <sub>3</sub>	16% @ 200 μM	4.72 ± 5.55
rac-19e	4-methoxyphenyl	H	CH <sub>3</sub>	CH <sub>3</sub>	H	CH <sub>3</sub>	27% @ 200 μM	14.6 ± 9.24
19f <sup>a</sup>	phenyl	H	H	H	H	H	12% @ 200 μM	16.8 ± 4.96
rac-19g	4-biphenyl	H	CH <sub>3</sub>	CH <sub>3</sub>	H	CH <sub>3</sub>	14% @ 200 μM	33.0 ± 13.8
19h	4-biphenyl	H	H	CH <sub>3</sub>	H	CH <sub>3</sub>	29% @ 200 μM	164.5 ± 23.4
19i	4-biphenyl	H	H	C <sub>2</sub> H <sub>5</sub>	H	C <sub>2</sub> H <sub>5</sub>	10% @ 200 μM	31% @ 50 μM
19j	2-methylphenyl	H	H	CH <sub>3</sub>	H	CH <sub>3</sub>	14% @ 200 μM	52% @ 50 μM
19k	4-methoxyphenyl	H	H	CH <sub>3</sub>	H	CH <sub>3</sub>	n.i. @ 200 μM	48% @ 50 μM
19l	4-methoxyphenyl	H	H	C <sub>2</sub> H <sub>5</sub>	H	C <sub>2</sub> H <sub>5</sub>	17% @ 200 μM	48% @ 50 μM
19m	4-chlorophenyl	H	H	C <sub>6</sub> H <sub>5</sub>	H	C <sub>6</sub> H <sub>5</sub>	11% @ 200 μM	46% @ 50 μM
rac-19n	4-methoxyphenyl	H	CH <sub>3</sub>	C <sub>2</sub> H <sub>5</sub>	H	C <sub>2</sub> H <sub>5</sub>	18% @ 200 μM	40% @ 50 μM
19o	4-chlorophenyl	H	H	C <sub>2</sub> H <sub>5</sub>	H	C <sub>2</sub> H <sub>5</sub>	18% @ 200 μM	38% @ 50 μM
19p	2-methylphenyl	H	H	H	H	H	11% @ 200 μM	n.i. @ 50 μM
19q	3-methylphenyl	H	H	C <sub>2</sub> H <sub>5</sub>	H	C <sub>2</sub> H <sub>5</sub>	n.i. @ 200 μM	n.i. @ 50 μM

<sup>a</sup>Compounds previously published by our group<sup>30</sup>

<sup>b</sup>n.i.: inhibition @ conc. [μM] < 10%

Analyzing the data of Table 2, we can confirm the findings of our preliminary SAR model,<sup>30</sup>

highlighting the importance of the 4,6-dimethylpyrimidine moiety for the binding of the ligand to

1  
2  
3 the newly formed 'selectivity pocket'. On the one hand, we show that ligands lose their affinity  
4 without the methyl groups at the pyrimidine ring in position 4 and/or 6 (**14j-l**), on the other hand  
5 we reveal that a higher degree of methylation (**14m**) or bulkier substituents (**14c**, **19l**, **19n-o**)  
6 cause a decrease in potency, as predicted by molecular docking studies (Figure 2d). Furthermore,  
7 we could show that polar substituents at the pyrimidine ring, e.g. -OH or -NH<sub>2</sub> (**14q-r**), are not  
8 beneficial in terms of potency. The inhibition data of the novel ligands with 2-naphthyl (**14n**),  
9 biphenyl (**19g-i**) or substituted phenyl moieties (**19a-e**, **19j-q**), which were generated to study the  
10 impact of structural changes of the arylmethyl moiety, clearly indicates the superiority of the 1-  
11 naphthyl substituted SirReals. We were able to rationalize the observed loss of *in vitro* potency  
12 caused by replacing the 1-naphthyl moiety with other aryl substituents e.g. biphenyl, by means of  
13 docking studies. These indicate a steric clash with the residues Val233, Phe234 and Phe235 of  
14 the binding pocket (data not shown). Comparing the substituted phenyl ligands with their parent  
15 compound **9**, we conclude that a substitution in position 3 is beneficial in terms of hSirt2  
16 inhibition (**19a-b**), whereas other substitution patterns lead to a decrease in potency (e.g. **19c-d**,  
17 **19j**). This observation is reflected by the docking results (Table S1) where we propose that the 4-  
18 position of the phenyl ring is unfavorable for substitution due to the close proximity of Phe234,  
19 whereas in the 3-position the substituent protrudes into the acyl-lysine channel (not shown). As  
20 predicted by molecular docking, an alkylation in the  $\alpha$ -position of the amide leads to increased  
21 potency of the (*S*)-enantiomer in the case of the methyl group (**(S)-14b**). Compared to *rac*-**14b**,  
22 an ethyl group already led to a decrease in potency (*rac*-**14h**). As the ethyl compounds (*rac*-**14h**,  
23 *rac*-**14f**) additionally turned out to be poorly soluble, we therefore did not separate the  
24 enantiomers of those compounds. Most importantly, however, we improved the *in vitro* activity  
25 of our lead structure by a chlorination or bromination of the naphthyl residue in position 7 (**14a**,  
26  
27  
28  
29  
30  
31  
32  
33  
34  
35  
36  
37  
38  
39  
40  
41  
42  
43  
44  
45  
46  
47  
48  
49  
50  
51  
52  
53  
54  
55  
56  
57  
58  
59  
60



1  
2  
3 **14d**). We were able to rationalize these results by binding free energy studies in combination  
4 with molecular docking (See Methods section for further details). Using docking poses  
5 calculated with the program GLIDE (Schrödinger LLC, New York, USA) and subsequent  
6 refinement using the program AMBER and a GBSA solvation model implemented in MOE  
7  
8 2012.10 (Chemical Computing Group, Montreal, Canada) we observed a correlation between the  
9  
10 experimental pIC<sub>50</sub> values and the calculated binding energies E<sub>GBSA</sub> (r<sup>2</sup>=0.67, RMSE 0.60,  
11  
12 q<sup>2</sup><sub>LOO</sub>=0.62, Figure S1). An improvement of the model was derived by including two topological  
13  
14 descriptors describing the ligand structures (“diameter” and surface descriptor “PEOE\_VSA4”,  
15  
16 see Methods section). The resulting model showed the following equation:  
17  
18  
19  
20  
21  
22  
23

$$24 \text{ pIC}_{50} = -1.474 - 0.192 \text{ “diameter”} - 0.032 \text{ “PEOE\_VSA4”} - 0.195 \text{ “E}_{\text{GBSA}}”$$

25  
26  
27 “Diameter” is the largest value in the distance matrix dimension of the molecules and is an  
28  
29 indicator of the dimension of the molecules. Increasing the “diameter” of the inhibitors is  
30  
31 unfavorable as well as increasing the surface descriptor “PEOE\_VSA4”. The final quantitative  
32  
33 structure activity relationship (QSAR) model is able to rationalize the observed *in vitro* activities  
34  
35 of the developed inhibitors (r<sup>2</sup>=0.81, RMSE 0.45, q<sup>2</sup><sub>LOO</sub>=0.76, Figure S2). The QSAR model was  
36  
37 further tested by 10-fold cross validation using randomly selected 20% of the compounds as test  
38  
39 set. The calculated q<sup>2</sup><sub>L20%O</sub> value of 0.74 supports the robustness of the model.  
40  
41  
42

43 Moreover, we were able to rationalize these results with a crystal structure of hSirt2 in complex  
44  
45 with **14d** and NAD<sup>+</sup> (Figure 3).  
46  
47  
48  
49  
50  
51  
52  
53  
54  
55  
56  
57  
58  
59  
60

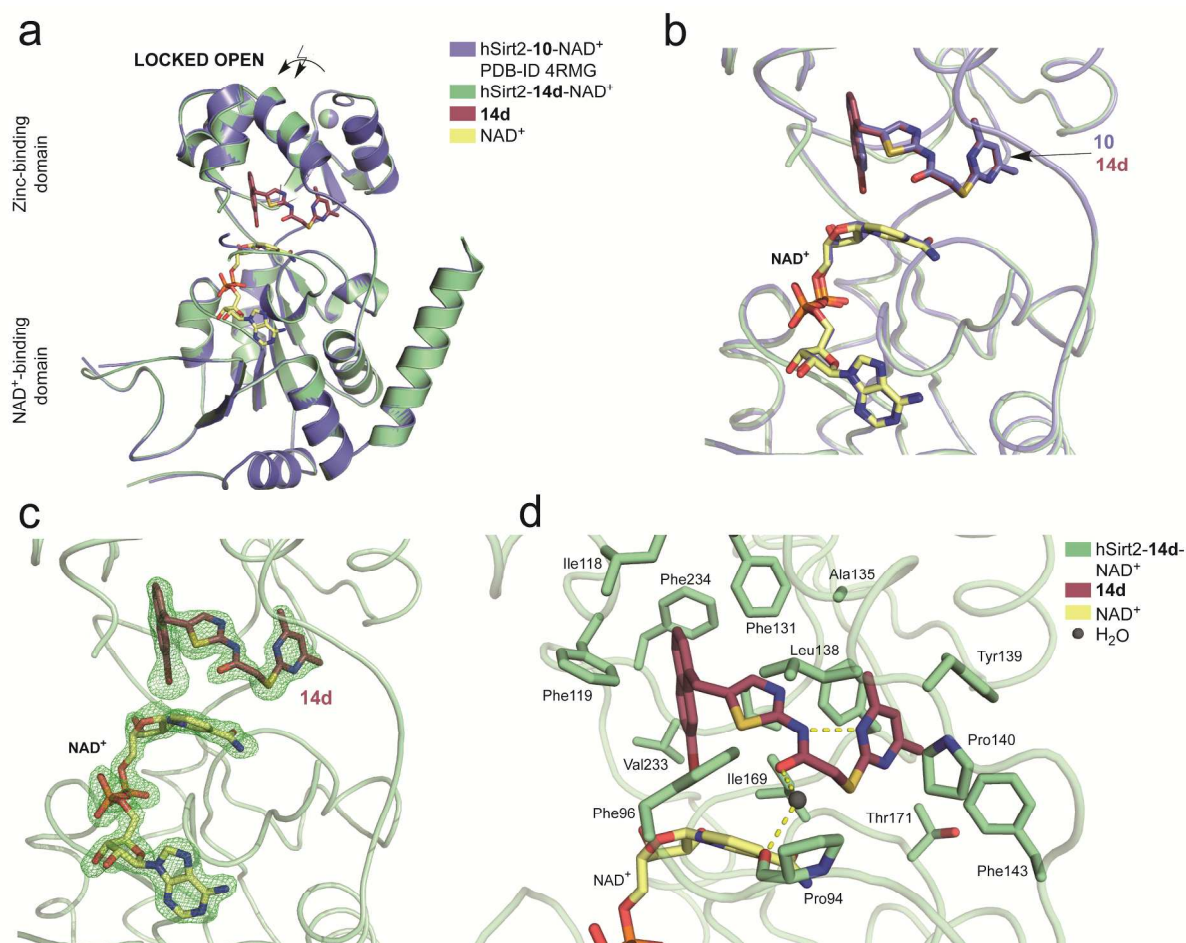


**Figure 3.** **14d** of the hSirt2-**14d**-NAD<sup>+</sup> complex binds to hSirt2 in a similar fashion as observed for **10** of the hSirt2-**10**-NAD<sup>+</sup> complex. (a) Superposition of the hSirt2-**10**-NAD<sup>+</sup> complex (cartoon: slate blue, PDB-ID 4RMG) with the crystal structure of hSirt2-**14d**-NAD<sup>+</sup> (cartoon: pale green; **14d**: raspberry sticks; NAD<sup>+</sup>: pale yellow sticks). Both complexes adopt the 'locked open'-conformation (RMSD of all C $\alpha$ -atoms: 0.33 Å). (b) **14d** and NAD<sup>+</sup> of the hSirt2-**14d**-NAD<sup>+</sup> complex assume a very similar position within the active site of hSirt2 as **10** and NAD<sup>+</sup> of the hSirt2-**10**-NAD<sup>+</sup> structure. (c) **14d** as well as NAD<sup>+</sup> are well-defined by the electron density.  $\sigma$ -weighted iterative OMIT maps are shown as green mesh and contoured at 3.0 $\sigma$ . (d) Interactions of **14d** with hSirt2. Interacting residues are represented as sticks (green). Phe190,

1  
2  
3 Ile232 are not labeled and Leu206 is not shown for the sake of clarity. The water molecule is  
4 represented as a black sphere and hydrogen bonds as dashes yellow lines.  
5  
6  
7

8  
9 The crystal structure reveals that **14d**, as well as  $\text{NAD}^+$ , assume a very similar position within the  
10 active site of hSirt2 compared to **10** and  $\text{NAD}^+$  of the hSirt2-**10**- $\text{NAD}^+$  structure (Figure 3a-b).  
11  
12 We were not able to observe a  $\sigma$ -hole interaction in our co-crystal structure as suggested by the  
13 docking study. Binding of **14d** is mainly driven by hydrophobic interactions with the side chains  
14 of the residues forming the extended C-site (ECS), the acyl-lysine binding site as well as the  
15 ‘selectivity pocket’ at the hinge region. The 7-bromonaphthyl substituent fills the lipophilic  
16 naphthyl binding site more efficiently than the unsubstituted naphthyl moiety, and thereby allows  
17 further hydrophobic interactions. The carbonyl-O of the amide also forms a water-mediated  
18 hydrogen bond to the backbone carbonyl-O of Pro94. As it was already observed in the crystal  
19 structure of hSirt2-**10**- $\text{NAD}^+$ , **14d** also forms an intramolecular hydrogen bond between the  
20 amide N-H and one of the nitrogen atoms of the dimethylpyrimidine ring. (Figure 3d). To see,  
21 whether the combination of beneficial substitution patterns would lead to a further increase in  
22 potency, we combined a 7-chloro substituent with an  $\alpha$ -methylation in the amide part. Yet, we  
23 did not detect an additive effect by combining a 7-halonaphthyl moiety with a methylation in the  
24  $\alpha$ -position of the amide (*rac*-**14i**).  
25  
26  
27  
28  
29  
30  
31  
32  
33  
34  
35  
36  
37  
38  
39  
40  
41  
42  
43  
44  
45  
46  
47  
48  
49  
50  
51  
52  
53  
54  
55  
56  
57  
58  
59  
60

To assess the cellular activity of the 7-halonaphthyl derivatives, we utilized immunofluorescence microscopy and western blot experiments, showing an enhanced tubulin hyperacetylation for **14a**, when compared to DMSO control (Figure 4, for raw images see Figure S3, for western blots Figure S4).

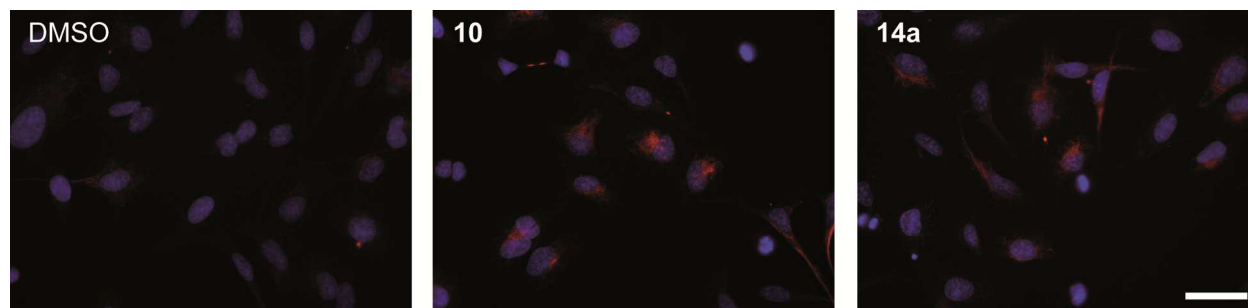


**Figure 4.** Optimized aminothiazole **14a** induces tubulin hyperacetylation in cultured HeLa cells. Acetylation level of the microtubule network (red) in the presence or absence of sirtuin inhibitors (10  $\mu\text{M}$ ). Treatment of HeLa cells with **14a** leads to higher acetylation levels of the microtubule network as compared to the DMSO treated cells (negative control). **10** was used as a positive control. Nuclei were DAPI-stained (blue). The scale bar represents 10  $\mu\text{m}$ .

Treatment with the optimized SirReal derivative **14a** leads to hyperacetylation of the microtubule network in a similar manner as observed for **10**, which was used as a positive control. While compounds **14a** and **10** both lead to a significant increase in tubulin hyperacetylation at a concentration of 20  $\mu\text{M}$ , **14a** also induces a significant gain in tubulin acetylation at only 10  $\mu\text{M}$  (Figure S4). Thus, we could show that the improved *in vitro* potency of **14a** is also relevant under physiological conditions. Of note, the halogenated derivatives were badly soluble in cell culture media and may therefore be limited in their efficacy at higher concentrations.

1  
2  
3 DISCUSSION AND CONCLUSION: Starting out from compounds **9** and **10** as potent and  
4 selective hSirt2 inhibitors, we established a synthesis platform to systematically probe the limits  
5 of modification within this scaffold. We were able to elaborate a well-defined SAR model for  
6 both, the arylmethyl and the pyrimidine moiety. Guided by the structural knowledge, revealed by  
7 hSirt2-**9/10** co-crystals as well as molecular docking studies, we were able to improve the *in*  
8 *vitro* hSirt2 inhibition of both lead structures, **9** and **10**. Moreover, the cellular activity of the  
9 improved aminothiazole inhibitor **14a** was validated by tubulin hyperacetylation in HeLa cells.  
10 In combination with the herein reported co-crystal structure, our SAR model will be the  
11 foundation for further developments of the Sirtuin Rearranging Ligands as valuable biological  
12 tool compounds to gain deeper insight into sirtuin biology and to probe the druggability of  
13 sirtuins.  
14  
15  
16  
17  
18  
19  
20  
21  
22  
23  
24  
25  
26  
27  
28  
29  
30  
31  
32  
33  
34  
35  
36  
37  
38  
39  
40  
41  
42  
43  
44  
45  
46  
47  
48  
49  
50  
51  
52  
53  
54  
55  
56  
57  
58  
59  
60

## EXPERIMENTAL SECTION:

**1. Protein expression and purification:** hSirt1<sub>133-747</sub> was expressed as a GST-tagged enzyme and purified as described previously.<sup>40</sup> hSirt2<sub>25-389</sub> was expressed N-terminally tagged with His<sub>6</sub><sup>41</sup> with minor modifications.<sup>40</sup> hSirt2<sub>56-356</sub> was expressed and purified according to Rumpf et al.<sup>30</sup>

**2. In Vitro Testing:** Potency of hSirt1 and hSirt2 inhibition was determined with a fluorescence-based homogeneous assay using the substrate ZMAL (Cbz-Lys(acetyl)-AMC).<sup>38</sup> hSirt1<sub>133-747</sub> or hSirt2<sub>25-389</sub> were mixed with assay buffer (50 mM Tris, 137 mM NaCl, 2.7 mM KCl, pH 8.0), NAD<sup>+</sup> (final assay concentration 500 μM), the substrate ZMAL (final assay concentration 10,5 μM), the inhibitor dissolved in DMSO at different concentrations, or DMSO only as a control (final DMSO concentration 5% (v/v)). To ensure initial state conditions, total substrate conversion of controls was adjusted to approximately 15% - 30%. The assay was performed in 96-well plates with a reaction volume of 60 μL per well. All determinations were performed at least in duplicates. After an incubation of 4 h at 37 °C and 140 rpm, deacetylation reaction was stopped by the addition of 60 μL of a stop solution containing trypsin and nicotinamide (50 mM Tris, 100 mM NaCl, 6.7% (v/v) DMSO, trypsin 5.5 U μL<sup>-1</sup>, 8 mM nicotinamide, pH 8.0). The reaction mixture was further incubated for 20 min at 37 °C and 140 rpm. Fluorescence intensity was measured in a microplate reader (BMG Polarstar, λ<sub>ex</sub> = 390 nm, λ<sub>em</sub> = 460 nm). Rates of inhibition were determined by using the controls, containing no inhibitor, as a reference. Graphpad Prism software (La Jolla, CA) was employed to determine IC<sub>50</sub> values.

**3. Data collection, structure solution and refinement:** Data were collected at 100 K at X06SA beamline of the Swiss Light Source (Villigen, Switzerland) equipped with a Pilatus 6M detector at a wavelength of 1.0 Å with oscillations of 0.5°. Data were processed with XDS<sup>42</sup> and scaled based on the CC1/2 criterion<sup>43</sup> using Aimless.<sup>44</sup> Data collection statistics are shown in Table 5.

The structure was solved by molecular replacement with MOLREP<sup>45</sup> using the hSirt2-10-NAD<sup>+</sup>-complex (PDB-ID 4RMG)<sup>30</sup> as a search model. The structural model was built in Coot<sup>46</sup> and refined with REFMAC.<sup>47</sup> **14d** was generated with the Grade Web Server (Global Phasing Ltd., United Kingdom) and placed into  $2F_o-F_c$  electron density maps using AFITT-CL (Version 2.1.0, OpenEye Scientific Software, Inc., Santa Fe, NM, USA.). All residues except Pro99, Ser100 and Thr101 were included in the model. The N-terminal glycine, histidine and methionine originate from the TEV cleavage site and the *NdeI*-restriction site of the modified pET15b- expression vector. The structure was validated using the Molprobit server<sup>48</sup> and PROCHECK.<sup>49</sup>  $\sigma$ -weighted iterative OMIT maps were generated with Phenix.<sup>50</sup> RMSD values were determined with SUPERPOSE<sup>51</sup> and images were prepared with Pymol (The Pymol Molecular Graphics System, Version 1.7, Schrödinger, LLC).

**Table 5.** Data collection and refinement statistics

	<b>hSirt2-14d-NAD<sup>+</sup></b>
<b>Data processing</b>	
PDB accession #	5DY4
Spacegroup	<i>I</i> 2
<i>a, b, c</i> (Å)	84.30, 55.43, 96.18
$\alpha, \beta, \gamma$ (°)	90, 114.91, 90
Resolution (Å)	46.78–1.77 (1.81–1.77)
Unique observations	38622 (2201)
Observations	260647 (15296)
Completeness (%)	98.2 (98.1)
Multiplicity	6.7 (6.9)
$R_{\text{merge}}$ <sup>[1]</sup>	0.095 (2.050)
<i>I</i> / $\sigma I$	10.3 (1.0)
CC1/2	0.998 (0.554)

<b>Refinement</b>	
Resolution (Å)	46.78–1.77 (1.81–1.77)
No. Amino acids	300
No. Atoms	2649
Protein	2391
<b>14d</b>	30
NAD <sup>+</sup>	44
Waters	183
Zn <sup>2+</sup>	1
R <sub>cryst</sub> /R <sub>free</sub> (%) <sup>[2]</sup>	17.5/21.3
<b>B factors (Å<sup>2</sup>)</b>	
Protein	33.71
<b>14d</b>	27.88
NAD <sup>+</sup>	29.05
Waters	38.64
Zn <sup>2+</sup>	27.58
RMSD bond length (Å)	0.013
RMSD angles (°)	1.65
<b>Ramachandran plot statistics</b>	
Most favoured region (%)	93.2
Additional allowed region (%)	6.5
Generously allowed region (%)	0.3
Disallowed region (%)	0.0

Values in parentheses represent the highest resolution shell.

$$^{[1]} R_{\text{merge}} = \sum_{\text{hkl}} [(\sum_i |I_i - \langle I \rangle|) / \sum_i I_i]$$

$$^{[2]} R_{\text{cryst}} = \sum_{\text{hkl}} ||F_{\text{obs}}| - |F_{\text{calc}}|| / \sum_{\text{hkl}} |F_{\text{obs}}|$$

R<sub>free</sub> is the cross-validation R factor computed for a test set of 5 % of unique reflections selected randomly.<sup>52</sup> Ramachandran statistics as defined by PROCHECK.<sup>49</sup>

**4. Protein crystallization:** Crystallization assays were set up with the Oryx Nano pipetting robot (Douglas Instruments, United Kingdom) using the vapor diffusion sitting drop method (Intelli-Plate 96-3 Low Profile, Art Robbins Instruments, USA) at 4 °C. Prior to crystallization, hSirt2<sub>56</sub>.



1  
2  
3  
4 356 (20 mg mL<sup>-1</sup>) was incubated with **14d** (100 mM stock solution in DMSO, 1% (v/v) final  
5  
6 DMSO concentration) and NAD<sup>+</sup> (100 mM stock solution in 25 mM Tris/HCl, 150 mM NaCl,  
7  
8 pH 8.0, final concentration 10 mM, Sigma-Aldrich, Germany). Crystals of the hSirt2-**14d**-  
9  
10 complex were obtained after 2 days in a solution containing 27% (w/v) PEG 3350 in 0.05 M  
11  
12 HEPES buffer at pH 7.0 with a protein solution to reservoir ratio of 3:1. The crystal was  
13  
14 mounted on a nylon loop and cryoprotected by the addition of 20% (v/v) glycerol.  
15  
16

17  
18 **5. Cell Culture:** HeLa (ATCC-2) cells were cultured in Dulbecco's Modified Eagle's Medium  
19  
20 (high glucose) supplemented with 10% (v/v) fetal calf serum, 100 µg/ml kanamycin (all reagents  
21  
22 from Sigma-Aldrich) in a humidified incubator at 37 °C with 5% CO<sub>2</sub>. For microscopic analysis,  
23  
24 0.5 x 10<sup>4</sup> cells were seeded on 12 mm diameter coverslips placed in 24-well plates and incubated  
25  
26 overnight before the experiment. For immunoblotting, 1.5 x 10<sup>4</sup> cells were seeded per well of 24-  
27  
28 well plates and incubated overnight. The drugs were added to cells for 1 hour from 10 mM stock  
29  
30 solutions in DMSO. Controls contained the corresponding amount of vehicle (DMSO).  
31  
32

33  
34 **6. Immunoblotting:** For the detection of acetylated tubulin, total tubulin and glyceraldehyde-3-  
35  
36 phosphate dehydrogenase (GAPDH) levels in cellular samples, we kept the cells at 37 °C and  
37  
38 washed them with prewarmed PBS. Next, the cells were lysed in 100 µL 1x reducing sample  
39  
40 buffer containing protein inhibitor mix and 2 mM EDTA (Sigma-Aldrich). Samples were  
41  
42 centrifuged at 10,000 g at 4°C for 5 min and the supernatants were stored at -70 °C. Samples  
43  
44 were analyzed by SDS-PAGE and blotted onto polyvinylidene difluoride membrane (Millipore).  
45  
46 The blot was developed sequentially using a monoclonal mouse antibody against acetylated  
47  
48 alpha-tubulin at Lys-40 (1:5000, clone 6-11B-1), than using a monoclonal mouse antibody  
49  
50 against alpha-tubulin (1:5000, clone DM1A), next using a monoclonal mouse antibody against  
51  
52 GAPDH (1 µg/mL, CB1001, clone 6C5, Calbiochem). Antibodies were detected by anti-mouse  
53  
54  
55  
56  
57  
58  
59  
60

1  
2  
3 IgG-peroxidase conjugate (Fc-specific), (1:5000, Sigma-Aldrich). Peroxidase reaction detected  
4  
5 using Immobilon Western substrate (Millipore) by a Bio-Rad ChemiDoc MP Imaging system  
6  
7 and its ImageLab 4.1 software. Intensity of spots was analysed by ImageJ 1.49 using Measure  
8  
9 command and subtracting background values. The sample values were normalized by the  
10  
11 average control value on the corresponding blot.  
12  
13

14  
15 **7. Immunofluorescence microscopy:** Immunofluorescence microscopy was performed as  
16  
17 previously reported.<sup>30</sup>  
18  
19

20  
21 **8. Computational Methods:** 3D structures of all compounds in this study were generated from  
22  
23 SMILES strings, and a subsequent energy minimization was carried out using the MMFF94x  
24  
25 force field implemented in Molecular Operating Environment System (MOE) 2012.10  
26  
27 (Chemical Computing Group, Montreal, Canada). All compounds were used in the protonation  
28  
29 state at physiological level. A maximum of 100 conformations were generated for each ligand  
30  
31 using the Conformational Search module implemented in MOE. All protein structures were  
32  
33 prepared by using the Structure Preparation module in MOE. Hydrogen atoms were added and  
34  
35 the protonation state for titratable amino acids was calculated using the Protonate 3D module in  
36  
37 MOE. Protein structures were energy minimized using the AMBER99 force field<sup>53</sup> with a  
38  
39 tethering force constant of  $(3/2) kT / 2$  ( $\sigma = 0.5 \text{ \AA}$ ) for all atoms during the minimization. AM1-  
40  
41 BCC charges were used for ligands.<sup>54</sup> All molecules except the zinc ion were removed from the  
42  
43 structures. Protein-ligand docking was performed using program GLIDE (Suite 2012-5.8,  
44  
45 Schrödinger LLC, New York, USA). The position of the inhibitor **10** in its crystal structure with  
46  
47 hSirt2/Ac-Lys-H3 peptide (PDB ID 4RMH) was used to define the size of the grid box (10 Å  
48  
49 radius). Docking was performed using GLIDE-Extra Precision (XP). The ligand was treated as  
50  
51 flexible and 20 docking poses were calculated for each inhibitor. All other options were left at  
52  
53  
54  
55  
56  
57  
58  
59  
60

1  
2  
3 their default values. The top-ranked pose from each docking run was included in the final  
4 analysis and viewed graphically together with the protein structure using the program MOE  
5  
6 2010.13 (Chemical Computing Group, Montreal, Canada). Using the docking setup, **10** could be  
7  
8 correctly docked into its crystal structure with RMSD values below 0.5 Å (PDB ID 4RMG and  
9  
10 4RMH).<sup>30</sup> Also, other active aminothiazole derivatives were predicted to adopt a similar binding  
11  
12 mode as was observed for **10**. Binding free energies for the inhibitors in this study were  
13  
14 calculated using the top-ranked docking poses. Structurally conserved water molecules included  
15  
16 for docking studies were maintained during the geometry optimization of the complexes. The  
17  
18 protein-inhibitor complexes were energy minimized using the AMBER PFROSST force field and  
19  
20 the GBSA solvation model implemented in MOE 2012.10. Using the resulting  $\Delta E_{\text{GBSA}}$  value as  
21  
22 descriptor, a significant correlation to the  $\text{pIC}_{50}$  values was observed ( $r^2=0.67$ ,  $\text{RMSE}=0.60$ ) for  
23  
24 the 30 compounds for which an  $\text{IC}_{50}$  and exact stereochemistry was determined (Figure S1).  
25  
26 Besides the correlation coefficient  $r^2$ , the model was also tested using leave one out (LOO) cross-  
27  
28 validation ( $q^2_{\text{LOO}}=0.62$ ). Furthermore, we investigated the effect of other descriptors like ligand  
29  
30 charge, diameter, or polar surface descriptors for establishing a QSAR model. We successfully  
31  
32 applied this approach recently for establishing predictive models with high robustness.<sup>55</sup> Among  
33  
34 192 tested 2D descriptors in MOE, the “diameter” and the topological surface descriptor  
35  
36 “PEOE\_VSA+4” showed the highest correlation. A QSAR model based on three descriptors,  
37  
38 namely “ $\Delta E_{\text{GBSA}}$  score”, “diameter”, and “PEO\_VSA+4” using MOE PLS methodology was  
39  
40 generated and validated. The final PLS model yielded a correlation coefficient of  $r^2=0.81$   
41  
42 (RMSE=0.45) and a  $q^2_{\text{LOO}}$  of 0.76 demonstrating the robustness of the model (Figure S2, Table  
43  
44 S1). Since LOO cross-validation is sometimes misleading and resulting in too optimistic models,  
45  
46 a more demanding cross-validation procedure was applied for the QSAR model. 10-fold cross  
47  
48  
49  
50  
51  
52  
53  
54  
55  
56  
57  
58  
59  
60

1  
2  
3 validation was carried out using randomly selected compounds (20%) as test set. Repeating this  
4  
5 random splitting 10 times, resulted in a mean  $q^2_{L20\%O}$  value of 0.74, demonstrating the  
6  
7 robustness of the model. All results are summarized in Table S2 in the Supplementary  
8  
9 Information.

10  
11  
12 **9. Chemistry:** Starting materials and reagents were obtained from commercial suppliers and  
13  
14 used without further purification. Thin-layer chromatography (TLC) for reaction monitoring was  
15  
16 performed with alumina plates coated with Merck silica gel 60 F<sub>254</sub> (layer thickness: 0.2 mm)  
17  
18 and analyzed under UV-light (254 nm). A mixture of ethyl acetate and cyclohexane (2:1) was  
19  
20 used as mobile phase. If the purity of the synthesized compounds was not adequate, we  
21  
22 performed flash column chromatography with TELOS Flash-LL Silica Columns 60M (0.040-  
23  
24 0.063 mm, 230-400 mesh) as a stationary phase on a Biotage Isolera One automated flash  
25  
26 purification system with UV-Vis detector. Cyclohexane and ethyl acetate was used as mobile  
27  
28 phase and gradient was adjusted based on TLC results. Yields were not optimized. <sup>1</sup>H-NMR and  
29  
30 <sup>13</sup>C-NMR spectra were recorded on Bruker Avance III HD spectrometer at 400 MHz and 100  
31  
32 MHz. The spectra are referenced against the NMR solvents and are reported as follows: <sup>1</sup>H:  
33  
34 chemical shift  $\delta$  (ppm), multiplicity (s = singlet, d = doublet, dd = doublet of doublets, t = triplet,  
35  
36 q = quartet, quint = quintet, sex = sextet, m = multiplet, b = broad), integration, coupling  
37  
38 constant (J in Hz). <sup>13</sup>C: chemical shift  $\delta$  (ppm), abbreviations: (q) = quaternary carbons,  
39  
40 quaternary carbons that could not be found in <sup>13</sup>C spectra but in HMBC or HSQC are  
41  
42 additionally marked with an asterisk (\*). The assignment resulted from HMBC and HSQC  
43  
44 experiments. Purity was determined for all tested compounds by HPLC and UV detection ( $\lambda$  =  
45  
46 210 nm) and was > 95%. HPLC analysis was performed using the following conditions: Eluent  
47  
48 A: H<sub>2</sub>O containing 0.05% TFA, Eluent B: acetonitrile containing 0.05% TFA, Eluent C: n-  
49  
50  
51  
52  
53  
54  
55  
56  
57  
58  
59  
60

1  
2  
3 hexane, Eluent D: propan-2-ol, flow rate 1 mL min<sup>-1</sup>. Method 1.1 (M1.1), analytical column,  
4 Phenomenex Synergi<sup>TM</sup> 4 μm MAX-RP 80 Å, 150 x 4.6 mm, isocratic conditions (A = 55%, B =  
5  
6 45%). Method 1.2 (M1.2), analytical column, Phenomenex Synergi<sup>TM</sup> 4 μm HYDRO-RP 80 Å,  
7  
8 250 x 4.6 mm. Method 1.3 (M1.3), analytical column, Phenomenex Synergi<sup>TM</sup> 4 μm POLAR-RP  
9  
10 80 Å, 150 x 4.6 mm. Method 2.1 (M2.1), analytical column, Phenomenex Synergi<sup>TM</sup> 4 μm  
11  
12 MAX-RP 80 Å, 150 x 4.6 mm, isocratic conditions (A = 40%, B = 60%). Method 2.2 (M2.2),  
13  
14 analytical column, Phenomenex Synergi<sup>TM</sup> 4 μm POLAR-RP 80 Å, 150 x 4.6 mm. Method 3  
15  
16 (M3), analytical column, Phenomenex Synergi<sup>TM</sup> 4 μm HYDRO-RP 80 Å, 250 x 4.6 mm,  
17  
18 isocratic conditions (A = 30%, B = 70%). Method 4 (M4), analytical column, Phenomenex  
19  
20 Synergi<sup>TM</sup> 4 μm HYDRO-RP 80 Å, 250 x 4.6 mm, isocratic conditions (A = 65%, B = 35%).  
21  
22 Method 5 (M5), analytical column, Phenomenex Synergi<sup>TM</sup> 4 μm HYDRO-RP 80 Å, 250 x 4.6  
23  
24 mm, isocratic conditions (A = 5%, B = 95%). Method 6.1 (M6.1), analytical column,  
25  
26 Phenomenex Synergi<sup>TM</sup> 4 μm HYDRO-RP 80 Å, 250 x 4.6 mm, linear gradient conditions (0–4  
27  
28 min, A = 90%, B = 10%; 4–29 min, linear increase to 100 % of B; 29–31 min, B = 100%; 31–40  
29  
30 min, A = 10%, B = 90%). Method 6.2 (M6.2), analytical column, Phenomenex Synergi<sup>TM</sup> 4 μm  
31  
32 MAX-RP 80 Å, 150 x 4.6 mm. Method 6.3 (M6.3), analytical column, Phenomenex Synergi<sup>TM</sup>  
33  
34 4 μm HYDRO-RP 80 Å, 250 x 4.6 mm. Method 7 (M7), analytical column, Phenomenex Lux<sup>TM</sup>  
35  
36 5 μm CELLULOSE-1, 250 x 4.6 mm, linear gradient conditions (0–4 min, C = 90%, D = 10%;  
37  
38 4–30 min, linear increase to C = 50%, D = 50%; 30–36 min, linear gradient to C=90%, D=10%,  
39  
40 36–40 min C=90%, D=10%. Melting temperatures were determined in glass capillary tubes with  
41  
42 the Stuart Melting Point Apparatus SMP2. Optical rotation was measured with a PerkinElmer  
43  
44 Model 341 Polarimeter. Mass spectra with electrospray ionization (ESI) were recorded on an  
45  
46 Advion expression CMS spectrometer, with electron ionization (EI) on an Agilent Technologies  
47  
48  
49  
50  
51  
52  
53  
54  
55  
56  
57  
58  
59  
60

6890 N Network GC-MS system. The synthesis of compounds **16e**,<sup>35a</sup> **22b**,<sup>36</sup> **23b**,<sup>37</sup> **33**,<sup>56</sup> has already been reported. Due to changes in the experimental procedure and to show unpublished characterization data, we have outlined the synthesis and the characterization data for those compound as well.

General Procedure for the Synthesis of 1,3,4-Thiadiazol-2-amines (**11a-e**):<sup>31</sup> A well-stirred mixture of thiosemicarbazide (1 equiv, 25 mmol), the carboxylic acid (1.2 equiv), and 8 mL of concentrated sulphuric acid was slowly heated to 80 – 90 °C and maintained at this temperature for 7 hours. After cooling, the reaction mixture was poured into ice water and was treated with concentrated ammonia to pH = 12. The crude product, which precipitated upon the addition of the ammonia, was filtered off and washed with water.

5-(1-Naphthylmethyl)-1,3,4-thiadiazol-2-amine (**11b**):<sup>57</sup> From thiosemicarbazide and 1-naphthylacetic acid. Yield: 3% of a beige solid.  $R_f$ : 0.15;  $^1\text{H-NMR}$  (DMSO- $\text{D}_6$ ,  $\delta$  [ppm]): 8.16-8.09 (m, 1H, naphthyl H-8), 7.98-7.92 (m, 1H, naphthyl H-5), 7.90-7.82 (m, 1H, naphthyl H-4), 7.60-7.43 (m, 4H, naphthyl H-2,3,6,7), 6.97 (bs, 2H, -NH<sub>2</sub>), 4.62 (s, 2H, Ar-CH<sub>2</sub>-Ar);  $^{13}\text{C-NMR}$  (DMSO- $\text{D}_6$ ,  $\delta$  [ppm]): 169.01 q (aminothiadiazole C-2), 158.20 q (aminothiadiazole C-5), 134.54 q (naphthyl C-1), 133.93 q (naphthyl C-4a), 131.66 q (naphthyl C-8a), 128.99 (naphthyl C-5), 128.18 (naphthyl C-4), 127.53 (naphthyl C-2), 126.74 (naphthyl C-7), 126.32 (naphthyl C-6), 126.11 (naphthyl C-3), 124.30 (naphthyl C-8), 33.80 (Ar-CH<sub>2</sub>-Ar); ESI-MS(+): 242.1 [M+H]<sup>+</sup>

General Procedure for Acylation of Thiazol-2-amines and 1,3,4-Thiadiazol-2-amines to generate amides (**12a-g**, **17a-j**, **18a-i**, **24a-b**, **31**, **37**, **43**, **44**):<sup>32</sup> To a solution of the amine (1 equiv, 2 mmol), dissolved in 10-30 mL acetonitrile, N,N-diisopropylethylamine (1.5 equiv) was added. The mixture was stirred and cooled to 0 °C. The acyl chloride (1.5 equiv) was

1  
2  
3 gradually added with stirring and cooling. After stirring for 2 h at room temperature, volatiles  
4  
5 were evaporated. The red brown, oily residue was mixed with water (10-30 mL) and precipitates  
6  
7 were collected by filtration. Precipitates were washed with water, hydrochloric acid (1 M), water,  
8  
9 and dried to yield the corresponding amide.  
10  
11

12  
13 2-Chloro-N-[5-[(7-chloro-1-naphthyl)methyl]thiazol-2-yl]acetamide (**17f**): From **15d** and  
14  
15 2-chloroacetyl chloride. Yield: 98% of a beige solid;  $R_f$ : 0.75;  $^1\text{H-NMR}$  (DMSO- $\text{D}_6$ ,  $\delta$  [ppm]):  
16  
17 12.32 (bs, 1H, amide-NH), 8.19 (d, 1H,  $^4J = 2.07$  Hz, naphthyl H-8), 8.01 (d, 1H,  $^3J = 8.85$  Hz,  
18  
19 naphthyl H-5), 7.91-7.88 (m, 1H, naphthyl H-4), 7.56-7.49 (m, 3H, naphthyl H-2,3,6), 7.34-7.32  
20  
21 (m, 1H, aminothiazole H-4), 4.59 (s, 2H, Ar- $\text{CH}_2$ -Ar), 4.32 (s, 2H,  $-\text{CH}_2\text{-Cl}$ );  $^{13}\text{C-NMR}$   
22  
23 (DMSO- $\text{D}_6$ ,  $\delta$  [ppm]): 165.13 q (amide-C), 156.67 q (aminothiazole C-2), 136.02 q (naphthyl  
24  
25 C-1), 135.38 (aminothiazole C-4), 132.35 (naphthyl-C4a), 132.22 q (naphthyl C-8a), 132.00 q  
26  
27 (aminothiazole C-5), 131.45 q (naphthyl C-7), 131.29 (naphthyl C-5), 128.26 (naphthyl C-2),  
28  
29 127.79 (naphthyl C-4), 126.81 (naphthyl C-3), 126.70 (naphthyl C-6), 123.24 (naphthyl C-8),  
30  
31 42.62 ( $-\text{CH}_2\text{-Cl}$ ), 29.60 (Ar- $\text{CH}_2$ -Ar); ESI-MS(-): 349.0  $[\text{M-H}]^-$   
32  
33  
34  
35

36  
37 General Procedure for S-Alkylation to generate Thioethers (**13a-h**, **14a-k**, **14m-o**, **14q-r**,  
38  
39 **19a-e**, **19g-q**, **20a**, **20c-d**, **26a-b**, **28-30**, **32**)<sup>32</sup> The aromatic thiol (1 equiv, 0.5 mmol) was  
40  
41 dissolved in 2 mL of DMSO.  $\text{Na}_2\text{CO}_3$  (2 equiv) and KI (1 equiv) were added. The mixture was  
42  
43 stirred for 15 min at room temperature. Then, the alkyl chloride (1 equiv) was added to the  
44  
45 reaction mixture and stirred for 2 h. After completion, water (10 mL) was added. The aqueous  
46  
47 layer was extracted with ethyl acetate (3 x 20 mL). The combined organic layers were dried over  
48  
49  $\text{Na}_2\text{SO}_4$  and evaporated. If necessary, the product was purified by automated flash column  
50  
51 chromatography (cyclohexane/EtOAc: gradient).  
52  
53  
54  
55  
56  
57  
58  
59  
60

1  
2  
3 N-[5-[(7-Chloro-1-naphthyl)methyl]thiazol-2-yl]-2-(4,6-dimethylpyrimidin-2-yl)sulfanyl-  
4  
5 acetamide (**14a**): From **17f** and **33**. Yield: 66% of a beige solid; mp: 217-219 °C;  $R_f$ : 0.62;  
6  
7  $^1\text{H-NMR}$  (DMSO- $\text{D}_6$ ,  $\delta$  [ppm]): 12.20 (bs, 1H, amide-NH), 8.17 (d, 1H,  $^4\text{J} = 2.12$  Hz, naphthyl  
8  
9 H-8), 8.00 (d, 1H,  $^3\text{J} = 8.62$  Hz, naphthyl H-5), 7.88 (dd, 1H,  $^3\text{J} = 7.12$  Hz,  $^4\text{J} = 2.25$  Hz, naphthyl  
10  
11 H-4), 7.55-7.47 (m, 3H, naphthyl H-2,3,6), 7.30-7.28 (m, 1H, aminothiazole H-4), 6.93 (s, 1H,  
12  
13 pyrimidine H-5), 4.56 (s, 2H, Ar- $\text{CH}_2$ -Ar), 4.05 (s, 2H,  $-\text{CH}_2$ -S-Ar), 2.26 (s, 6H,  
14  
15 pyrimidine  $-\text{CH}_3$ );  $^{13}\text{C-NMR}$  (DMSO- $\text{D}_6$ ,  $\delta$  [ppm]): 169.28 q (pyrimidine C-2), 167.38 q  
16  
17 (pyrimidine C-4,6), 167.24 q (amide-C), 157.09 q (aminothiazole C-2), 136.08 q (naphthyl C-1),  
18  
19 135.32 (aminothiazole C-4), 132.34 q (naphthyl C-4a), 132.23 q (naphthyl C-8a), 131.41 q  
20  
21 (aminothiazole C-5), 131.35 q (naphthyl C-7), 131.27 (naphthyl C-2), 128.23 (naphthyl C-5),  
22  
23 127.74 (naphthyl C-4), 126.77 (naphthyl C-6), 126.66 (naphthyl C-3), 123.24 (naphthyl C-8),  
24  
25 116.50 (pyrimidine C-5), 34.43 ( $-\text{CH}_2$ -S-Ar), 29.64 (Ar- $\text{CH}_2$ -Ar), 23.61 (pyrimidine  $-\text{CH}_3$ );  
26  
27 Purity: 99.3% (11.28 min, M2.2); ESI-MS(+): 477.1 [M+Na] $^+$   
28  
29  
30  
31  
32  
33

34 General Procedure for the Synthesis of 5-(Arylmethyl)thiazol-2-amines (**15a-f**, **16g**):<sup>35</sup> The  
35  
36 aromatic amine (1 equiv, 20 mmol) was dissolved in a minimal amount of aqueous hydrochloric  
37  
38 acid (2 M) under heating. The mixture was vigorously stirred and cooled to  $-5 - 0$  °C. The  
39  
40 hydrochloride partially precipitates. Then, a cooled and acidified solution of  $\text{NaNO}_2$  (2.5 M, 1  
41  
42 equiv) was added dropwise. The reaction mixture was stirred for 10 min at  $-5 - 0$  °C.  $\text{FeCl}_3 \times 6$   
43  
44  $\text{H}_2\text{O}$  (3 equiv) was dissolved in a minimal amount of  $\text{H}_2\text{O}$  and added to the generated yellow  
45  
46 colored arenediazonium chloride solution. Concentrated hydrochloric acid was given to the  
47  
48 stirred reaction mixture until arenediazonium tetrachloroferrate(II) precipitated quantitatively.  
49  
50 The temperature was maintained at  $-5 - 0$  °C. The precipitated salt was filtered off and dried. A  
51  
52 solution of  $\text{CuCl}_2 \times 2 \text{H}_2\text{O}$  (0.5 equiv) in 23 mL of ethanol and 1.5 mL of concentrated  
53  
54  
55  
56  
57  
58  
59  
60



1  
2  
3 hydrochloric acid was added at -5 - 0 °C to a solution of the arenediazonium  
4 tetrachloroferrate(II) (1 equiv) in 30 mL of acetone. The precipitate of arenediazonium  
5 tetrachlorocuprate(II) was filtered off, washed with diethyl ether, and dried under reduced  
6 pressure. An additional amount of the salt was precipitated from the filtrate by adding 50 mL of  
7 diethyl ether. The arenediazonium tetrachlorocuprate(II) was gradually added in portions to  
8 acrolein (2.5 equiv) dissolved in 40 mL of aqueous acetone (1:1 (v/v)) while stirring at room  
9 temperature. After the evolution of nitrogen has stopped, water (50 mL) was added. Diethyl ether  
10 was added to extract the  $\alpha$ -chloropropanal from the aqueous layer. Combined organic layers  
11 were dried over Na<sub>2</sub>SO<sub>4</sub> and solvents were evaporated. The crude  $\alpha$ -chloropropanal (1 equiv)  
12 was dissolved in ethanol (20 mL), and thiourea (1.6 g, 21 mmol) was added. The reaction  
13 mixture was heated under reflux for 2 h. After cooling to room temperature, water (100 mL) was  
14 added and the mixture was neutralized with ammonia. The aqueous layer was extracted with  
15 ethyl acetate (3 x 100 mL). The combined organic layers were dried over Na<sub>2</sub>SO<sub>4</sub> and volatiles  
16 were evaporated. The brown crude product was purified by automated flash column  
17 chromatography (cyclohexane/EtOAc: gradient) to yield the aminothiazole.

18  
19  
20  
21  
22  
23  
24  
25  
26  
27  
28  
29  
30  
31  
32  
33  
34  
35  
36  
37  
38  
39 5-[(7-Chloro-1-naphthyl)methyl]thiazol-2-amine (**15d**): From **21b**. Yield: 25% of a beige  
40 solid;  $R_f$ : 0.27; <sup>1</sup>H-NMR (DMSO-D<sub>6</sub>,  $\delta$  [ppm]): 8.16 (d, 1H, <sup>4</sup>J = 2.00 Hz, naphthyl H-8), 7.99  
41 (d, 1H, <sup>3</sup>J = 8.81 Hz, naphthyl H-5), 7.88-7.84 (m, 1H, naphthyl H-4), 7.53 (dd, 1H, <sup>3</sup>J = 8.81 Hz,  
42 <sup>4</sup>J = 2.00 Hz, naphthyl H-6), 7.51-7.45 (m, 2H, naphthyl H-2,3), 6.75-6.72 (m, 1H, aminothiazole  
43 H-4), 6.69 (bs, 2H, -NH<sub>2</sub>), 4.37 (s, 2H, -CH<sub>2</sub>-); <sup>13</sup>C-NMR (DMSO-D<sub>6</sub>,  $\delta$  [ppm]): 168.14 q  
44 (aminothiazole C-2), 136.46 q (naphthyl C-1), 136.07 (aminothiazole C-4), 132.30 q (naphthyl  
45 C-8a), 132.28 q (naphthyl C-4a), 131.26 q (naphthyl C-7), 131.21 (naphthyl C-5), 127.92  
46  
47  
48  
49  
50  
51  
52  
53  
54  
55  
56  
57  
58  
59  
60

1  
2  
3 (naphthyl C-2), 127.51 (naphthyl C-3), 126.69 (naphthyl C-6), 126.64 (naphthyl C-4), 124.63 q  
4  
5 (aminothiazole C-5), 123.28 (naphthyl C-8), 30.16 (-CH<sub>2</sub>-); ESI-MS(+): 275.1 [M+H]<sup>+</sup>  
6  
7

8 General Procedure for the Synthesis of 5-(Arylmethyl)thiazol-2-amines (**16a-f**):<sup>35a</sup> The aniline  
9 derivative (1 equiv, 20 mmol) was dissolved in a minimal amount of aqueous hydrochloric acid  
10 (2 M) under heating. The mixture was vigorously stirred and cooled to -5 – 0 °C. The  
11 hydrochloride partially precipitates. Then, a cooled and acidic solution of NaNO<sub>2</sub> (2.5 M, 1  
12 equiv) was added dropwise to the reaction mixture. The reaction mixture was incubated for 10  
13 min at -5 – 0 °C. In the synthesis of **16b-e** the generated yellow colored arenediazonium chloride  
14 solution was preliminary neutralized with NaHCO<sub>3</sub> to a pH of 6-7, and MgO (0.25 equiv) was  
15 added to the mixture. The acidic (**16a, 16f**) or neutralized (**16b-e**) solution of the arenediazonium  
16 chloride was added dropwise to a flask, which was loaded with acrolein (1 equiv), CuCl<sub>2</sub> x 2  
17 H<sub>2</sub>O (0.3 equiv), and 5 mL of acetone. The reaction mixture was stirred at room temperature  
18 until the evolution of nitrogen stopped. Then, the organic layer was separated, and the aqueous  
19 layer was extracted with diethyl ether. The organic layer was combined with the extracts, dried  
20 over Na<sub>2</sub>SO<sub>4</sub>, and solvents were removed under reduced pressure. The crude α-chloropropanal  
21 (1 equiv) was dissolved in ethanol (20 mL) and thiourea (1.6 g, 21 mmol) was added. The  
22 reaction mixture was heated under reflux for 2 h. After cooling to room temperature, water  
23 (100 mL) was added and the mixture was neutralized with ammonia. The aqueous layer was  
24 extracted with ethyl acetate (3 x 100 mL). The combined organic layers were dried over Na<sub>2</sub>SO<sub>4</sub>  
25 and volatiles were evaporated. The brown crude product was purified by automated flash column  
26 chromatography (cyclohexane/EtOAc: gradient) to yield the aminothiazole.  
27  
28  
29  
30  
31  
32  
33  
34  
35  
36  
37  
38  
39  
40  
41  
42  
43  
44  
45  
46  
47  
48  
49  
50  
51

52 5-(m-Tolylmethyl)thiazol-2-amine (**16e**): From 3-methylaniline as previously reported.<sup>35a</sup>  
53 Yield: 3% of a beige solid; *R<sub>f</sub>*: 0.28; <sup>1</sup>H-NMR (CDCl<sub>3</sub>, δ [ppm]): 7.25-7.19 (m, 1H, 3-tolyl H-5),  
54  
55  
56  
57  
58  
59  
60

1  
2  
3 7.10-7.02 (m, 3H, 3-tolyl H-2,4,6), 6.82-6.78 (m, 1H, aminothiazole H-4), 5.31 (bs, 2H, -NH<sub>2</sub>),  
4  
5 3.93 (s, 2H, Ar-CH<sub>2</sub>-Ar), 2.36 (s, 3H, 3-tolyl -CH<sub>3</sub>); <sup>13</sup>C-NMR (CDCl<sub>3</sub>, δ [ppm]): 167.83 q  
6  
7 (aminothiazole C-2), 139.71 q (3-tolyl C-1), 138.19 q (3-tolyl C-3), 135.31 (aminothiazole C-4),  
8  
9 129.10 (3-tolyl C-2), 128.43 (3-tolyl C-5), 127.76 q (aminothiazole C-5), 127.35 (3-tolyl C-4),  
10  
11 125.35 (3-tolyl C-6), 33.24 (Ar-CH<sub>2</sub>-Ar), 21.37 (3-tolyl -CH<sub>3</sub>); ESI-MS(+): 205.1 [M+H]<sup>+</sup>  
12  
13  
14

15  
16 General Procedure for the Reduction of Nitronaphthalenes to generate Naphthalenamines  
17  
18 (**21a-c**): The nitronaphthalene (1 equiv, 12 mmol) and SnCl<sub>2</sub> x 2 H<sub>2</sub>O were suspended in 100 mL  
19  
20 of ethanol. The reaction mixture was stirred for 4 - 24 h at room temperature. After completion,  
21  
22 the solvent was evaporated, and residues were suspended in 1 L of NaOH (1 M). The product  
23  
24 was extracted with ethyl acetate (3 x 200 mL). Combined organic layers were dried over Na<sub>2</sub>SO<sub>4</sub>  
25  
26 and evaporated under reduced pressure. The crude product was purified by automated flash  
27  
28 column chromatography (cyclohexane/EtOAc: gradient).  
29  
30

31  
32 7-Chloronaphthalen-1-amine (**21b**): From **23b**. Yield: 65% of a purple solid; *R<sub>f</sub>*: 0.90;  
33  
34 <sup>1</sup>H-NMR (CDCl<sub>3</sub>, δ [ppm]): 7.84 (d, 1H, <sup>4</sup>J = 1.93 Hz, H-8), 7.76 (d, 1H, <sup>3</sup>J = 8.87 Hz, H-5), 7.42  
35  
36 (dd, 1H, <sup>3</sup>J = 8.87 Hz, <sup>4</sup>J = 1.93 Hz, H-6), 7.32-7.29 (m, 2H, H-3,4), 6.85-6.82 (m, 1H, H-2), 4.17  
37  
38 (bs, 2H, -NH<sub>2</sub>); <sup>13</sup>C-NMR (CDCl<sub>3</sub>, δ [ppm]): 141.25 q (C-1), 132.55 q (C-4a), 130.63 q (C-7),  
39  
40 130.09 (C-5), 126.63 (C-6), 126.57 (C-3), 124.31 q (C-8a), 120.20 (C-8), 118.83 (C-4), 110.76  
41  
42 (C-2); ESI-MS(-): 176.1 [M-H]<sup>-</sup>  
43  
44

45  
46 Synthesis of Nitronaphthalenamines (**22a-b**):<sup>36</sup> Concentrated sulfuric acid (120 mL) was  
47  
48 cooled to -5 to -10 °C and treated slowly with 2-aminonaphthalene-1-sulfonic acid (1 equiv, 70.5  
49  
50 mmol) under vigorous stirring. Most of the 2-aminonaphthalene-1-sulfonic acid was soluble and  
51  
52 the liquid was cooled to -15 °C. Dry powdered potassium nitrate (1 equiv) was added. The  
53  
54 brown solution was stirred for 40 min at this temperature and then poured onto 0.5 kg of ice. The  
55  
56  
57  
58  
59  
60

precipitate was filtered off, washed, and then extracted with a cold diluted sodium carbonate solution. The filtered extracts were cooled to 5 °C and acidified with concentrated hydrochloric acid. After 2 h on ice, a mixture of mono-nitrated 2-aminonaphthalene-1-sulfonic acids was filtered off, washed with ice water, and dried. The reaction yielded 9.65g (95%) of a tan crystalline powder. Without further purification, the mixture of mono-nitrated 2-aminonaphthalene-1-sulfonic acids was suspended in 140 mL of 45% sulfuric acid and refluxed for 40 min. The hot mixture was diluted to 2 L with water and an aqueous solution of sodium hydroxide was added to a basic pH. The suspension was cooled to 10 °C for 1.5 h, and the precipitated material was filtered off, washed with water, and dried. The structural isomers were separated by automated flash column chromatography (cyclohexane/EtOAc: gradient).

8-Nitronaphthalen-2-amine (**22b**): Yield: 27% of a deep red solid;  $R_f$ : 0.86;  $^1\text{H-NMR}$  (DMSO- $\text{D}_6$ ,  $\delta$  [ppm]): 8.18 (dd, 1H,  $^3\text{J} = 7.84$  Hz,  $^4\text{J} = 1.26$  Hz, naphthyl H-7), 8.06-8.00 (m, 1H, naphthyl H-5), 7.80 (d, 1H,  $^3\text{J} = 8.87$  Hz, naphthyl H-4), 7.54 (d, 1H,  $^4\text{J} = 2.29$  Hz, naphthyl H-1), 7.18 (t, 1H,  $^3\text{J} = 7.84$  Hz, naphthyl H-6), 7.08 (dd, 1H,  $^3\text{J} = 8.87$  Hz,  $^4\text{J} = 2.29$  Hz, naphthyl H-3), 6.19 (s, 2H,  $-\text{NH}_2$ );  $^{13}\text{C-NMR}$  (DMSO- $\text{D}_6$ ,  $\delta$  [ppm]): 151.33 q (naphthyl C-2), 143.12 q (naphthyl C-8), 135.64 (naphthyl C-5), 130.84 (naphthyl C-4), 128.12 q (naphthyl C-4a), 127.75 q (naphthyl C-8a), 125.70 (naphthyl C-7), 119.65 (naphthyl C-3), 118.95 (naphthyl C-6), 101.12 (naphthyl C-1); ESI-MS(-): 187.1 [M-H] $^-$ .

General Procedure for the Synthesis of Halonitronaphthalenes (**23a-c**):<sup>37</sup> The respective nitronaphthylamine (1 equiv, 32.6 mmol) was dissolved in 33 mL of glacial acid. A solution of sodium nitrite (1.7 equiv) dissolved in 33 mL of concentrated sulfuric acid was added gradually with stirring, the temperature was kept at 15-20 °C. After another 15 min, the arenediazonium salt solution was added dropwise while stirring to a solution of freshly prepared cuprous(I)

1  
2  
3 halogenide (4 equiv) dissolved in 50 mL of concentrated hydrochloric acid (for **23a-b**), or  
4 hydrobromic acid (for **23c**). After the termination of nitrogen evolution, water was added to the  
5  
6 reaction mixture to precipitate the product quantitatively. Precipitates were filtered off, washed  
7  
8 with aqueous NaOH (2 M) and water.  
9  
10

11  
12 7-Chloro-1-nitro-naphthalene (**23b**): From **22b** and CuCl dissolved in concentrated  
13 hydrochloric acid. Yield: 58% of a pale yellow solid;  $R_f$ : 0.88;  $^1\text{H-NMR}$  ( $\text{CDCl}_3$ ,  $\delta$  [ppm]): 8.69  
14 (d, 1H,  $^4J = 1.95$  Hz, H-8), 8.34 (dd, 1H,  $^3J = 7.80$  Hz,  $^4J = 1.18$  Hz, H-2), 8.16-8.11 (m, 1H, H-  
15 4), 7.93 (d, 1H,  $^3J = 8.79$  Hz, H-5), 7.60 (dd, 1H,  $^3J = 8.79$  Hz,  $^4J = 1.95$  Hz, H-6), 7.59 (t, 1H,  $^3J$   
16 = 7.80 Hz, H-3);  $^{13}\text{C-NMR}$  ( $\text{CDCl}_3$ ,  $\delta$  [ppm]): 145.39 q (C-1), 136.12 q (C-7), 134.67 (C-4),  
17 132.55 q (C-4a), 130.08 (C-5), 128.49 (C-6), 125.74 q (C-8a), 125.27 (C-2), 124.43 (C-3),  
18 122.52 (C-8); EI-MS(-): 207 [M]<sup>-</sup>  
19  
20  
21  
22  
23  
24  
25  
26  
27  
28

29 2-Mercapto-4,6-dimethylpyrimidine (**33**)<sup>56</sup> as an Example for the General Procedure for the  
30 Synthesis of 2-Mercaptoprimidines: Thiourea (1 equiv, 26 mmol) and acetylacetone (1.5 equiv)  
31 were dissolved in ethanol. During cooling and stirring, 2.5 mL of concentrated sulfuric acid were  
32 added to the flask. After 48 h of stirring at room temperature, the reaction mixture was heated to  
33 a slight boiling under reflux for 30 min. After cooling to room temperature, the yellow  
34 crystalline mass was filtered off, washed with ice-cold ethanol, and dried under reduced pressure.  
35 The yellow solid was solved in a minimal amount of water. Barium carbonate was added to a  
36 neutral reaction. The clear filtrate from the barium salts was then evaporated to dryness. The  
37 crude product was recrystallized from ethanol. Yield: 39% of a yellow solid;  $R_f$ : 0.08;  $^1\text{H-NMR}$   
38 (DMSO- $\text{D}_6$ ,  $\delta$  [ppm]): 13.40 (bs, 1H, -SH), 6.62 (s, 1H, 5-H), 2,25 (s, 6H, -CH<sub>3</sub>);  $^{13}\text{C-NMR}$   
39 (DMSO- $\text{D}_6$ ,  $\delta$  [ppm]): 181.67 q (C-2), 164.58 q (C-4,6); 110.16 (C-5); 21,71 (-CH<sub>3</sub>); ESI-MS(+):  
40 141.1 [M+H]<sup>+</sup>  
41  
42  
43  
44  
45  
46  
47  
48  
49  
50  
51  
52  
53  
54  
55  
56  
57  
58  
59  
60

## ASSOCIATED CONTENT

**Supporting Information.** Experimental details, spectral data for compounds **11a**, **11c-e**, **12a-g**, **13a-h**, **14b-k**, **14m-o**, **14q-r**, **15a-c**, **15e-f**, **16a-d**, **16f-g**, **17a-e**, **17g-j**, **18a-i**, **19a-e**, **19g-q**, **20a**, **20c-d**, **21a**, **21c**, **22a**, **23a**, **23c**, **24a-b**, **25**, **26a-b**, **27-32**, **34-47**, Tables S1-2, and Figures S1-4.

This material is available free of charge *via* the Internet at <http://pubs.acs.org>.

## AUTHOR INFORMATION

**Corresponding Author**

\* Phone: +497612034896. E-mail: [manfred.jung@pharmazie.uni-freiburg.de](mailto:manfred.jung@pharmazie.uni-freiburg.de).

**Funding Sources**

The studies have been supported by the Deutsche Forschungsgemeinschaft (Inhibitors: Ju295/8-1, Si868/6-1, structural work: SFB992 Medical Epigenetics, Project Z02). J. Ovádi was supported by the Hungarian National Scientific Research Fund Grants OTKA T-101039 and K-112144. J.O., W.S. and M.J. thank the COST Action CM1406 (EPIBIOCHEM) for support.

**Notes**

The authors declare no competing financial interest.

## ABREVIATIONS USED

AMC, 7-amino-4-methylcumarin; DIPEA, *N,N*-diisopropylethylamine; EtOAc, ethyl acetate; ECS, extended C-site; GAPDH, glyceraldehyde-3-phosphate dehydrogenase; HEPES, 4-(2-hydroxyethyl)-1-piperazineethanesulfonic acid; hSirt2, human sirtuin2; LOO, leave one out; MOE, molecular operating environment; RMSE, root mean square error; RP, reversed phase;

1  
2  
3 SirReal, sirtuin rearranging ligands; SMILES, simplified molecular input line entry specification;  
4  
5 ZMAL, Cbz-(acetyl)Lys-AMC;  
6  
7

8  
9 ACKNOWLEDGMENT

10  
11 We thank Karin Schmidtkunz for performing the tests for hSirt1 inhibition and Sascha Ferlaino  
12  
13 for NMR measurements.  
14

15  
16 REFERENCES

- 17  
18 1. de Ruijter, A. J.; van Gennip, A. H.; Caron, H. N.; Kemp, S.; van Kuilenburg, A. B.  
19  
20 Histone deacetylases (HDACs): characterization of the classical HDAC family. *Biochem. J.*  
21  
22 **2003**, *370*, 737-749.  
23  
24  
25  
26 2. Sauve, A. A. Sirtuin chemical mechanisms. *Biochim. Biophys. Acta* **2010**, *1804*, 1591-  
27  
28 1603.  
29  
30  
31  
32 3. Feldman, J. L.; Baeza, J.; Denu, J. M. Activation of the protein deacetylase SIRT6 by  
33  
34 long-chain fatty acids and widespread deacylation by mammalian sirtuins. *J. Biol. Chem.* **2013**,  
35  
36 288, 31350-31356.  
37  
38  
39  
40 4. Jiang, H.; Khan, S.; Wang, Y.; Charron, G.; He, B.; Sebastian, C.; Du, J.; Kim, R.; Ge,  
41  
42 E.; Mostoslavsky, R.; Hang, H. C.; Hao, Q.; Lin, H. SIRT6 regulates TNF-alpha secretion  
43  
44 through hydrolysis of long-chain fatty acyl lysine. *Nature* **2013**, *496*, 110-113.  
45  
46  
47  
48 5. Du, J.; Zhou, Y.; Su, X.; Yu, J. J.; Khan, S.; Jiang, H.; Kim, J.; Woo, J.; Kim, J. H.; Choi,  
49  
50 B. H.; He, B.; Chen, W.; Zhang, S.; Cerione, R. A.; Auwerx, J.; Hao, Q.; Lin, H. Sirt5 is a NAD-  
51  
52 dependent protein lysine demalonylase and desuccinylase. *Science* **2011**, *334*, 806-809.  
53  
54  
55  
56  
57  
58  
59  
60

- 1  
2  
3 6. North, B. J.; Marshall, B. L.; Borra, M. T.; Denu, J. M.; Verdin, E. The human Sir2  
4 ortholog, SIRT2, is an NAD<sup>+</sup>-dependent tubulin deacetylase. *Mol. Cell* **2003**, *11*, 437-444.  
5  
6  
7  
8  
9 7. Yeung, F.; Hoberg, J. E.; Ramsey, C. S.; Keller, M. D.; Jones, D. R.; Frye, R. A.; Mayo,  
10 M. W. Modulation of NF-kappaB-dependent transcription and cell survival by the SIRT1  
11 deacetylase. *EMBO J.* **2004**, *23*, 2369-2380.  
12  
13  
14  
15  
16  
17 8. Vaziri, H.; Dessain, S. K.; Ng Eaton, E.; Imai, S. I.; Frye, R. A.; Pandita, T. K.; Guarente,  
18 L.; Weinberg, R. A. hSIR2(SIRT1) functions as an NAD-dependent p53 deacetylase. *Cell* **2001**,  
19 *107*, 149-159.  
20  
21  
22  
23  
24  
25 9. North, B. J.; Rosenberg, M. A.; Jeganathan, K. B.; Hafner, A. V.; Michan, S.; Dai, J.;  
26 Baker, D. J.; Cen, Y.; Wu, L. E.; Sauve, A. A.; van Deursen, J. M.; Rosenzweig, A.; Sinclair, D.  
27 A. SIRT2 induces the checkpoint kinase BubR1 to increase lifespan. *EMBO J.* **2014**, *33*, 1438-  
28 1453.  
29  
30  
31  
32  
33  
34  
35 10. Du, J.; Jiang, H.; Lin, H. Investigating the ADP-ribosyltransferase activity of sirtuins  
36 with NAD analogues and <sup>32</sup>P-NAD. *Biochemistry* **2009**, *48*, 2878-2890.  
37  
38  
39  
40  
41 11. Haigis, M. C.; Guarente, L. P. Mammalian sirtuins - emerging roles in physiology, aging,  
42 and calorie restriction. *Genes Dev.* **2006**, *20*, 2913-2921.  
43  
44  
45  
46 12. Verdin, E.; Hirsche, M. D.; Finley, L. W.; Haigis, M. C. Sirtuin regulation of  
47 mitochondria: energy production, apoptosis, and signaling. *Trends Biochem. Sci.* **2010**, *35*, 669-  
48 675.  
49  
50  
51  
52  
53  
54  
55  
56  
57  
58  
59  
60



- 1  
2  
3  
4  
5  
6  
7  
8  
9  
10  
11  
12  
13  
14  
15  
16  
17  
18  
19  
20  
21  
22  
23  
24  
25  
26  
27  
28  
29  
30  
31  
32  
33  
34  
35  
36  
37  
38  
39  
40  
41  
42  
43  
44  
45  
46  
47  
48  
49  
50  
51  
52  
53  
54  
55  
56  
57  
58  
59  
60
13. Liu, T. F.; Vachharajani, V. T.; Yoza, B. K.; McCall, C. E. NAD<sup>+</sup>-dependent sirtuin 1 and 6 proteins coordinate a switch from glucose to fatty acid oxidation during the acute inflammatory response. *J. Biol. Chem.* **2012**, *287*, 25758-25769.
14. Feige, J. N.; Auwerx, J. Transcriptional targets of sirtuins in the coordination of mammalian physiology. *Curr. Opin. Cell Biol.* **2008**, *20*, 303-309.
15. Schemies, J.; Uciechowska, U.; Sippl, W.; Jung, M. NAD(+) -dependent histone deacetylases (sirtuins) as novel therapeutic targets. *Med. Res. Rev.* **2010**, *30*, 861-889.
16. Beirowski, B.; Gustin, J.; Armour, S. M.; Yamamoto, H.; Viader, A.; North, B. J.; Michan, S.; Baloh, R. H.; Golden, J. P.; Schmidt, R. E.; Sinclair, D. A.; Auwerx, J.; Milbrandt, J. Sir-two-homolog 2 (Sirt2) modulates peripheral myelination through polarity protein Par-3/atypical protein kinase C (aPKC) signaling. *Proc. Natl. Acad. Sci. U S A* **2011**, *108*, E952-961.
17. de Oliveira, R. M.; Sarkander, J.; Kazantsev, A. G.; Outeiro, T. F. SIRT2 as a therapeutic target for age-related disorders. *Front. Pharmacol.* **2012**, *3*, 82.
18. (a) Pais, T. F.; Szego, E. M.; Marques, O.; Miller-Fleming, L.; Antas, P.; Guerreiro, P.; de Oliveira, R. M.; Kasapoglu, B.; Outeiro, T. F. The NAD-dependent deacetylase sirtuin 2 is a suppressor of microglial activation and brain inflammation. *EMBO J.* **2013**, *32*, 2603-2616; (b) Zhao, T.; Alam, H. B.; Liu, B.; Bronson, R. T.; Nikolian, V. C.; Wu, E.; Chong, W.; Li, Y. Selective inhibition of SIRT2 improves outcomes in a lethal septic model. *Curr. Mol. Med.* **2015**, *15*, 634-641; (c) Eskandarian, H. A.; Impens, F.; Nahori, M. A.; Soubigou, G.; Coppee, J. Y.; Cossart, P.; Hamon, M. A. A role for SIRT2-dependent histone H3K18 deacetylation in bacterial infection. *Science* **2013**, *341*, 1238858.

- 1  
2  
3 19. (a) Kim, H. S.; Vassilopoulos, A.; Wang, R. H.; Lahusen, T.; Xiao, Z.; Xu, X.; Li, C.;  
4 Veenstra, T. D.; Li, B.; Yu, H.; Ji, J.; Wang, X. W.; Park, S. H.; Cha, Y. I.; Gius, D.; Deng, C. X.  
5 SIRT2 maintains genome integrity and suppresses tumorigenesis through regulating APC/C  
6 activity. *Cancer Cell* **2011**, *20*, 487-499; (b) Yang, M. H.; Laurent, G.; Bause, A. S.; Spang, R.;  
7 German, N.; Haigis, M. C.; Haigis, K. M. HDAC6 and SIRT2 regulate the acetylation state and  
8 oncogenic activity of mutant K-RAS. *Mol. Cancer Res.* **2013**, *11*, 1072-1077.  
9  
10  
11  
12  
13  
14  
15  
16  
17  
18 20. Donmez, G.; Outeiro, T. F. SIRT1 and SIRT2: emerging targets in neurodegeneration.  
19 *EMBO Mol. Med.* **2013**, *5*, 344-352.  
20  
21  
22  
23  
24 21. Park, S. H.; Zhu, Y.; Ozden, O.; Kim, H. S.; Jiang, H.; Deng, C. X.; Gius, D.;  
25 Vassilopoulos, A. SIRT2 is a tumor suppressor that connects aging, acetylome, cell cycle  
26 signaling, and carcinogenesis. *Transl. Cancer Res.* **2012**, *1*, 15-21.  
27  
28  
29  
30  
31  
32 22. Lawson, M.; Uciechowska, U.; Schemies, J.; Rumpf, T.; Jung, M.; Sippl, W. Inhibitors to  
33 understand molecular mechanisms of NAD(+)-dependent deacetylases (sirtuins). *Biochim.*  
34 *Biophys. Acta* **2010**, *1799*, 726-739.  
35  
36  
37  
38  
39  
40 23. Cui, H.; Kamal, Z.; Ai, T.; Xu, Y.; More, S. S.; Wilson, D. J.; Chen, L. Discovery of  
41 potent and selective sirtuin 2 (SIRT2) inhibitors using a fragment-based approach. *J. Med. Chem.*  
42 **2014**, *57*, 8340-8357.  
43  
44  
45  
46  
47  
48 24. Suzuki, T.; Khan, M. N. A.; Sawada, H.; Imai, E.; Itoh, Y.; Yamatsuta, K.; Tokuda, N.;  
49 Takeuchi, J.; Seko, T.; Nakagawa, H.; Miyata, N. Design, synthesis, and biological activity of a  
50 novel series of human sirtuin-2-selective inhibitors. *J. Med. Chem.* **2012**, *55*, 5760-5773.  
51  
52  
53  
54  
55  
56  
57  
58  
59  
60

1  
2  
3  
4  
5  
6  
7  
8  
9  
10  
11  
12  
13  
14  
15  
16  
17  
18  
19  
20  
21  
22  
23  
24  
25  
26  
27  
28  
29  
30  
31  
32  
33  
34  
35  
36  
37  
38  
39  
40  
41  
42  
43  
44  
45  
46  
47  
48  
49  
50  
51  
52  
53  
54  
55  
56  
57  
58  
59  
60

25. Disch, J. S.; Evindar, G.; Chiu, C. H.; Blum, C. A.; Dai, H.; Jin, L.; Schuman, E.; Lind, K. E.; Belyanskaya, S. L.; Deng, J.; Coppo, F.; Aquilani, L.; Graybill, T. L.; Cuozzo, J. W.; Lavu, S.; Mao, C.; Vlasuk, G. P.; Perni, R. B. Discovery of thieno[3,2-d]pyrimidine-6-carboxamides as potent inhibitors of SIRT1, SIRT2, and SIRT3. *J. Med. Chem.* **2013**, *56*, 3666-3679.

26. Di Fruscia, P.; Zacharioudakis, E.; Liu, C.; Moniot, S.; Laohasinnarong, S.; Khongkow, M.; Harrison, I. F.; Koltsida, K.; Reynolds, C. R.; Schmidtkunz, K.; Jung, M.; Chapman, K. L.; Steegborn, C.; Dexter, D. T.; Sternberg, M. J. E.; Lam, E. W. F.; Fuchter, M. J. The Discovery of a highly selective 5,6,7,8-tetrahydrobenzo[4,5]thieno[ 2,3-d] pyrimidin-4(3H)-one SIRT2 inhibitor that is neuroprotective in an in vitro Parkinson's disease model. *ChemMedChem* **2015**, *10*, 69-82.

27. Outeiro, T. F.; Kontopoulos, E.; Altmann, S. M.; Kufareva, I.; Strathearn, K. E.; Amore, A. M.; Volk, C. B.; Maxwell, M. M.; Rochet, J. C.; McLean, P. J.; Young, A. B.; Abagyan, R.; Feany, M. B.; Hyman, B. T.; Kazantsev, A. G. Sirtuin 2 inhibitors rescue alpha-synuclein-mediated toxicity in models of Parkinson's disease. *Science* **2007**, *317*, 516-519.

28. (a) Lara, E.; Mai, A.; Calvanese, V.; Altucci, L.; Lopez-Nieva, P.; Martinez-Chantar, M. L.; Varela-Rey, M.; Rotili, D.; Nebbioso, A.; Ropero, S.; Montoya, G.; Oyarzabal, J.; Velasco, S.; Serrano, M.; Witt, M.; Villar-Garea, A.; Imhof, A.; Mato, J. M.; Esteller, M.; Fraga, M. F. Salermide, a Sirtuin inhibitor with a strong cancer-specific proapoptotic effect. *Oncogene* **2009**, *28*, 781-791; (b) Peck, B.; Chen, C. Y.; Ho, K. K.; Di Fruscia, P.; Myatt, S. S.; Coombes, R. C.; Fuchter, M. J.; Hsiao, C. D.; Lam, E. W. SIRT inhibitors induce cell death and p53 acetylation through targeting both SIRT1 and SIRT2. *Mol. Cancer Ther.* **2010**, *9*, 844-55.

- 1  
2  
3 29. Yamagata, K.; Goto, Y.; Nishimasu, H.; Morimoto, J.; Ishitani, R.; Dohmae, N.; Takeda,  
4 N.; Nagai, R.; Komuro, I.; Suga, H.; Nureki, O. Structural basis for potent inhibition of SIRT2  
5 deacetylase by a macrocyclic peptide inducing dynamic structural change. *Structure* **2014**, *22*,  
6 345-352.  
7  
8  
9  
10  
11  
12  
13 30. Rumpf, T.; Schiedel, M.; Karaman, B.; Roessler, C.; North, B. J.; Lehotzky, A.; Olah, J.;  
14 Ladwein, K. I.; Schmidtkunz, K.; Gajer, M.; Pannek, M.; Steegborn, C.; Sinclair, D. A.;  
15 Gerhardt, S.; Ovadi, J.; Schutkowski, M.; Sippl, W.; Einsle, O.; Jung, M. Selective Sirt2  
16 inhibition by ligand-induced rearrangement of the active site. *Nat. Commun.* **2015**, *6*, 6263.  
17  
18  
19  
20  
21  
22  
23 31. Chubb, F. L.; Nissenbaum, J. Some Hypoglycemic Thiadiazoles. *Can. J. Chem.* **1959**, *37*,  
24 1121-1123.  
25  
26  
27  
28  
29 32. Zav'yalov, S. I.; Kravchenko, N. E.; Ezhova, G. I.; Kulikova, L. B.; Zavozin, A. G.;  
30 Dorofeeva, O. V. Synthesis of 2-aminothiazole derivatives. *Pharm. Chem. J.* **2007**, *41*, 105-108.  
31  
32  
33  
34 33. Meerwein, H.; Büchner, E.; van Emster, K. Über die Einwirkung aromatischer  
35 Diazoverbindungen auf  $\alpha$ ,  $\beta$ -ungesättigte Carbonylverbindungen. *J. Prakt. Chem.* **1939**, *152*,  
36 237-266.  
37  
38  
39  
40  
41  
42 34. Bülow, C.; Sproesser, T. Über primäre Disazokombinationen des Benzyläthyl-m-  
43 amidophenols. *Ber. Dtsch. Chem. Ges.* **1908**, *41*, 1684-1692.  
44  
45  
46  
47  
48 35. (a) Obushak, N. D.; Matiichuk, V. S.; Vasylyshin, R. Y.; Ostapyuk, Y. V. Heterocyclic  
49 syntheses on the basis of arylation products of unsaturated compounds: X. 3-aryl.-2-  
50 chloropropanals as reagents for the synthesis of 2-amino-1,3-thiazole derivatives. *Russ. J. Org.*  
51 *Chem.* **2004**, *40*, 383-389; (b) Obushak, N. D.; Lyakhovich, M. B.; Bilaya, E. E. Arenediazonium  
52  
53  
54  
55  
56  
57  
58  
59  
60

1  
2  
3 tetrachlorocuprates(II). Modified versions of the Meerwein and Sandmeyer reactions. *Russ. J.*  
4  
5 *Org. Chem.* **2002**, *38*, 38-46.

6  
7  
8  
9 36. Morrison, D. C.; Lee, H. P. C. A new preparation of 8-Nitro-2-Naphthylamine. *J. Org.*  
10  
11 *Chem.* **1962**, *27*, 3336-3337.

12  
13  
14 37. Beech, W. F.; Legg, N. Aminohydroxynaphthoic acids .1. Synthesis of 6-amino-4-  
15  
16 hydroxy-2-naphthoic acid (carboxy gamma-acid). *J. Chem. Soc.* **1949**, 1887-1889.

17  
18  
19  
20 38. Heltweg, B.; Trapp, J.; Jung, M. In vitro assays for the determination of histone  
21  
22 deacetylase activity. *Methods* **2005**, *36*, 332-337.

23  
24  
25  
26 39. Kazantsev, A. G. Compositions and methods for modulating sirtuin activity, and  
27  
28 therapeutic use. U.S. Patent No. 20090259044, **2012**.

29  
30  
31 40. Neugebauer, R. C.; Uchiechowska, U.; Meier, R.; Hrubby, H.; Valkov, V.; Verdin, E.;  
32  
33 Sippl, W.; Jung, M. Structure-activity studies on splitomicin derivatives as sirtuin inhibitors and  
34  
35 computational prediction of binding mode. *J. Med. Chem.* **2008**, *51*, 1203-1213.

36  
37  
38  
39 41. North, B. J.; Schwer, B.; Ahuja, N.; Marshall, B.; Verdin, E. Preparation of enzymatically  
40  
41 active recombinant class III protein deacetylases. *Methods* **2005**, *36*, 338-345.

42  
43  
44 42. Kabsch, W., Xds. *Acta Crystallogr., Sect. D: Biol. Crystallogr.* **2010**, *66*, 125-132.

45  
46  
47  
48 43. Karplus, P. A.; Diederichs, K. Linking crystallographic model and data quality. *Science*  
49  
50 **2012**, *336*, 1030-1033.

51  
52  
53  
54 44. Winn, M. D.; Ballard, C. C.; Cowtan, K. D.; Dodson, E. J.; Emsley, P.; Evans, P. R.;  
55  
56 Keegan, R. M.; Krissinel, E. B.; Leslie, A. G. W.; McCoy, A.; McNicholas, S. J.; Murshudov, G.

1  
2  
3 N.; Pannu, N. S.; Potterton, E. A.; Powell, H. R.; Read, R. J.; Vagin, A.; Wilson, K. S. Overview  
4 of the CCP4 suite and current developments. *Acta Crystallogr., Sect. D: Biol. Crystallogr.* **2011**,  
5  
6 67, 235-242.  
7  
8

9  
10  
11 45. Vagin, A.; Teplyakov, A. Molecular replacement with MOLREP. *Acta Crystallogr., Sect.*  
12  
13 *D: Biol. Crystallogr.* **2010**, 66, 22-25.  
14

15  
16  
17 46. Emsley, P.; Lohkamp, B.; Scott, W. G.; Cowtan, K. Features and development of Coot.  
18  
19 *Acta Crystallogr., Sect. D: Biol. Crystallogr.* **2010**, 66, 486-501.  
20

21  
22 47. Murshudov, G. N.; Skubak, P.; Lebedev, A. A.; Pannu, N. S.; Steiner, R. A.; Nicholls, R.  
23  
24 A.; Winn, M. D.; Long, F.; Vagin, A. A. REFMAC5 for the refinement of macromolecular  
25  
26 crystal structures. *Acta Crystallogr., Sect. D: Biol. Crystallogr.* **2011**, 67, 355-367.  
27  
28

29  
30 48. Chen, V. B.; Arendall, W. B.; Headd, J. J.; Keedy, D. A.; Immormino, R. M.; Kapral, G.  
31  
32 J.; Murray, L. W.; Richardson, J. S.; Richardson, D. C. MolProbity: all-atom structure validation  
33  
34 for macromolecular crystallography. *Acta Crystallogr., Sect. D: Biol. Crystallogr.* **2010**, 66, 12-  
35  
36 21.  
37  
38

39  
40 49. Laskowski, R. A.; Macarthur, M. W.; Moss, D. S.; Thornton, J. M. Procheck - a Program  
41  
42 to Check the Stereochemical Quality of Protein Structures. *J. Appl. Crystallogr.* **1993**, 26, 283-  
43  
44 291.  
45  
46

47  
48 50. Adams, P. D.; Afonine, P. V.; Bunkoczi, G.; Chen, V. B.; Davis, I. W.; Echols, N.;  
49  
50 Headd, J. J.; Hung, L. W.; Kapral, G. J.; Grosse-Kunstleve, R. W.; McCoy, A. J.; Moriarty, N.  
51  
52 W.; Oeffner, R.; Read, R. J.; Richardson, D. C.; Richardson, J. S.; Terwilliger, T. C.; Zwart, P.  
53  
54  
55  
56  
57  
58  
59  
60

1  
2  
3 H. PHENIX: a comprehensive Python-based system for macromolecular structure solution. *Acta*  
4  
5  
6 *Crystallogr., Sect. D: Biol. Crystallogr.* **2010**, *66*, 213-221.

7  
8  
9 51. Krissinel, E. Fold Recognition Using Efficient Short Fragment Clustering. *J. Mol.*  
10  
11 *Biochem.* **2012**, *1*, 76-85

12  
13  
14 52. Brunger, A. T. Free R-value - a novel statistical quantity for assessing the accuracy of  
15  
16 crystal-structures. *Nature* **1992**, *355*, 472-475.

17  
18  
19 53. Wang, J. M.; Wolf, R. M.; Caldwell, J. W.; Kollman, P. A.; Case, D. A. Development  
20  
21 and testing of a general amber force field. *J. Comput. Chem.* **2004**, *25*, 1157-1174.

22  
23  
24 54. Jakalian, A.; Jack, D. B.; Bayly, C. I. Fast, efficient generation of high-quality atomic  
25  
26 charges. AM1-BCC model: II. Parameterization and validation. *J. Comput. Chem.* **2002**, *23*,  
27  
28 1623-1641.

29  
30  
31 55. Slynko, I.; Scharfe, M.; Rumpf, T.; Eib, J.; Metzger, E.; Schüle, R.; Jung, M.; Sippl, W.  
32  
33 Virtual screening of PRK1 inhibitors: Ensemble docking, rescoring using binding free energy  
34  
35 calculation and QSAR model development. *J. Chem. Inf. Model* **2014**, *54*, 138-150.

36  
37  
38 56. Hale, W. J.; Williams, A. G. The constitution of acetylacetone-thiourea. *J. Am. Chem.*  
39  
40 *Soc.* **1915**, *37*, 594-600.

41  
42  
43 57. Tan, T. F.; Li, Y. X.; Bai, L. G.; Wu, B. P.; Guo, H. Y.; Suo, Z. C. A facile synthesis and  
44  
45 optical properties of novel 2-substituted-5-naphthylmethylene thiadiazole derivatives. *Adv.*  
46  
47 *Mater. Res-Switz.* **2014**, *1052*, 188-192.

